Formation of Apollo 16 impactites and the composition of late accreted material: Constraints from Os isotopes, highly siderophile elements and sulfur abundances

Philipp Gleißner, Harry Becker

Freie Universität Berlin, Institut für Geologische Wissenschaften, Malteserstr. 74-100, 12249 Berlin, Germany

Received 22 August 2016; accepted in revised form 10 December 2016; Available online 18 December 2016

Geochimica et Cosmochimica Acta 200 (2017) 1–24 http://dx.doi.org/10.1016/j.gca.2016.12.017

Corresponding author: E-mail addresses: gleissner@zedat.fu-berlin.de

Abstract:

Fe-Ni metal-schreibersite-troilite intergrowths in Apollo 16 impact melt rocks and new highly siderophile element (HSE) and S abundance data indicate that millimeter-scale closed-system fractional crystallization processes during cooling of impactor-derived metal melt droplets in impact-melts are the main reason for compositional variations and strong differences in abundances and ratios of HSE in multiple aliquots from Apollo 16 impact melt rocks. Element ratios obtained from linear regression of such data are therefore prone to error, but weighted averages take into account full element budgets in the samples and thus represent a more accurate estimate of their impactor contributions. Modeling of solid metal-liquid metal partitioning in the Fe-Ni-S-P system and HSE patterns in impactites from different landing sites suggest that bulk compositions of ancient lunar impactites should be representative of impact melt compositions and that large-scale fractionation of the HSE by *in situ* segregation of solid metal or sulfide liquid in impact melt sheets most likely did not occur. The compositional record of lunar impactites indicates accretion of variable amounts of chondritic and non-chondritic impactor material and the mixing of these components during remelting of earlier ejecta deposits. The non-chondritic composition appears most prominently in some Apollo 16 impactites and is characterized by suprachondritic HSE/Ir ratios which increase from refractory to moderately volatile HSE and exhibit a characteristic enrichment of Ru relative to Pt. Large-scale fractional crystallization of solid metal from sulfur and phosphorous rich metallic melt with high P/S in planetesimal or embryo cores is currently the most likely process that may have produced these compositions. Similar materials or processes may have contributed to the HSE signature of the bulk silicate Earth (BSE).

Keywords: Lunar impactites; HSE; Late accretion

1. INTRODUCTION

The surface of the Moon is shaped by impact basins and craters of different sizes and the structure and composition of its crust is altered by a deep megaregolith formation and contaminated with impactor material. Ancient lunar impactites related to large basin-forming impacts which were formed prior to 3.8 Ga provide a unique record of material accreted after the lunar crust formation. Understanding the composition and source of the late impacting material has important implications for the inner solar system dynamics and the late accretion history of the terrestrial planets (e.g. Bottke et al., 2007, 2010; Walker et al., 2015).

Since core-mantle differentiation removes virtually all highly siderophile elements (HSE) from the silicate portion of differentiated bodies, these elements should be highly depleted in mantles and crusts of planetary bodies (e.g.

Mann et al., 2012). Therefore, the HSE record of ancient lunar impactites is assumed to be entirely dominated by the admixture of small proportions of impactors and thus may constrain their HSE composition (e.g. Morgan et al., 1977; Hertogen et al., 1977; Palme, 1980). Such data may also hold the key to understanding the observed excess abundance of HSE in the Earth's mantle and the slight deviation of some HSE ratios from chondritic ratios (Morgan et al., 2001; Becker et al., 2006).

Lunar impactites analyzed by neutron activation techniques revealed several distinguishable siderophile element compositions, some of which were slightly different from chondritic compositions (e.g. Morgan et al., 1972, 1974, 1977, 2001). Especially mafic impact melt rocks of the Apollo 16 landing site were found to display high metal abundances (1–2 vol.%), high abundances of HSE (5–30 ng/g Ir), and Au/Ir ratios more fractionated compared to other landing sites. Consequently, the involvement of a differentiated impactor component was suspected early on (e.g. the R-group of Ganapathy et al., 1973 and Krähenbühl et al., 1973; the 1H group of Hertogen et al., 1977). More complete and precise HSE concentration and osmium isotope data are now available, however, the distri- bution of HSE within samples and the origin of observed differences in composition between samples from different lithologies and landing sites are still being debated.

The use of relative abundances of the HSE in ancient lunar impact melt rocks as a fingerprint of meteoritic impactors was based on the assumption that large-scale fractionation of the HSE during impact and within the impact melts did not occur. However, this assumption has never been evaluated systematically. In the simplest case, the HSE budget of rocks, which upon impact were molten completely, is assumed to represent a two-component mixture of a HSE-rich impactor and HSE-poor lunar highland crust. In such a case, regression of HSE vs. Ir using multiple aliquots of the same rock should yield linear trends with slopes corresponding to the HSE/Ir ratio of the impactor. However, data scatter larger than analytical uncertainty, curved trends and non-zero y-intercepts of regression lines were observed and were interpreted to either reflect target contributions (Puchtel et al., 2008), modest fractionation of some HSE by volatilization or crystal fractionation within in the impact melt sheet (James et al., 2007; Fischer-Gö dde and Becker, 2012; Sharp et al., 2014) or sim- ply incomplete mixing of HSE carrier phases from impac- tors of different compositions (Liu et al., 2015).

Obtaining compositional constraints on impactors from ancient lunar impactites is important for our understanding of the nature of late accreted material. Despite the new data published in recent years, key questions that are still being debated concern whether or not the measured compositions and the correlation of element ratios with $^{187}Os/^{188}Os$ ratios (as a time-integrated measure of Re/Os) represent the compositions of specific impactors (Sharp et al., 2014), a mixing of several impactor compositions (Fischer-Gödde and Becker, 2012) or a fractionation trend due to large-scale fractional crystallization of metal within large impact melt pools, similar to terrestrial analogs (Vaughan et al., 2013). Consequently, the HSE record of ancient lunar impactites was interpreted to reflect late accretion of chondritic material, but possibly also primitive objects outside the range of known chondrites (Norman et al., 2002; Puchtel et al., 2008; Sharp et al., 2014; Liu et al., 2015). Alternatively, differentiated compositions like fragments of planetesimal cores were suggested (Morgan et al., 1972, 1974; Fischer-Gödde and Becker, 2012). A key feature of such ''non-chondritic" lunar impactites are suprachondritic Ru/Pt ratios. This type of fractionation was observed in some pallasites (Lee et al., 2006; Danielson et al., 2009) and occurs in experimental studies of the Fe-Ni-S-P system (Corrigan et al., 2009; Chabot et al., 2014).

Here, we report new $^{187}Os/^{188}Os$, HSE and sulfur concentration data of 56 subsamples of five Apollo 16 impact melt rocks. In order to test previous assumptions on the distribution of meteoritic components in impact melt rocks, we have obtained all concentration and isotope data from the same digestion aliquot of rock fragments or mineral separates, using isotope dilution (except for Rh and Au) combined with ICP-MS and N-TIMS techniques. In order to have a better evaluation of multi-aliquot analyses, we will focus on the influence of small-scale fractionation processes by using combined HSE + S concentration data to model solid metal-liquid metal fractionation processes during crystallization of the impact melts. The new data in combination with data from the literature will be used to evaluate the plausibility of large-scale fractionation processes in impact melt sheets and solid metal-liquid metal fractionation in the cores of parent bodies of putative impactors. We also assess mixing processes which may have produced the range of HSE compositions observed in ancient lunar impactites.

2. APOLLO 16 IMPACT MELT ROCKS

The Apollo 16 mission, initially planned to sample the central lunar highlands, returned mainly rock specimen which were either directly produced or heavily modified by impacts. Impacts large enough to melt a considerable portion of the target are believed to produce melt pools where molten target material and impactor mix to form impact melt sheets. Due to melting of feldspatic crustal target rocks including lower crustal lithologies, many impact melt rocks are very highly aluminous (VHA) and KREEP-rich (KREEP = rich in potassium, rare-earth ele- ments, phosphorus, and other alkali and high-field- strength elements), but at the same time overall basaltic in composition (Walker et al., 1973).

We studied five impact melt rocks: intersertal (62295, 195), intergranular (65055, 54), hyaloophitic (61016, 512), subophitic (64475, 110) and poikilitic (60335, 150). A detailed petrographic description, photographs of the rock fragments used in the present work and a summary of previous neutron activation data of lithophile and siderophile trace elements are given in the Electronic Supplement.

3. METHODS

All sample preparation, digestion, chemical separation and mass spectrometry work was done at Freie Universität

Berlin, Germany. In general, we followed the well-established techniques of Fischer-Gödde et al. (2010), Fischer-Gödde and Becker (2012) and Wang et al. (2013) developed for the analysis of terrestrial and extraterrestrial samples and standard materials.

3.1. Sample preparation and digestion

Samples were broken into coarse chips using an alumina ceramic mortar and pestle, exclusively used for lunar samples. In order to obtain pure impact melt material, if possible clasts were avoided. Opaque phases were separated whenever possible from the fine fraction of the broken sample, using a magnet covered by glass. In order to distinguish between different opaque phases, the latter were separated further according to their magnetic susceptibility. Strongly to weakly magnetic fractions are assumed to represent differences in chemical composition reflecting different steps of a crystallization sequence from predominantly Fe-Ni metal to metal-schreibersite-troilite intergrowths. Separated magnetic fractions were then treated as individual subsample.

For each sample, 8 to 15 subsamples of 60–190 mg (0.4–8 mg in case of metal separates) were weighed into quartz glass digestion vessels and mixed ^{185}Re–^{190}Os, ^{105}Pd–^{99}Ru-^{191}Ir–^{194}Pt–and ^{34}S spike solutions were added. Sample digestion was carried out in a high-pressure asher (Anton Paar™) using 3 ml reverse aqua regia at 10 MPa and 320 °C for 16 h.

3.2. Chemical separation

Osmium was separated by solvent extraction from reverse aqua regia into chloroform, directly after digestion. After back extraction into HBr the Os fraction was further purified by micro-distillation for 3 h at 85 °C into 15 µl HBr (Birck et al., 1997).

Rhenium, Ir, Ru, Pt, Rh, Pd and Au were separated by cation exchange chromatography using 10 ml pre-cleaned Eichrom™ 50W-X8 resin (100–200 mesh). In order to recover Rh and Au digestion solutions were converted into chloride form and then dissolved in 0.5 M HCl-60% acetone before loading onto the columns (Fischer-Gödde et al., 2010; Fischer-Gödde and Becker, 2012).

Sulfur was separated from 5% to 10% of the reverse aqua regia solution. The samples were taken to near dryness and then dissolved in 4 ml 0.1 M HNO_3. Sulfur was separated on 1 ml pre-cleaned Eichrom™ 50W-X8 resin (100–200 mesh).

3.3. Mass spectrometry

The purified Os was loaded on baked Pt-filaments and covered with NaOH-$Ba(OH)_2$ solution. The isotopic composition was measured by negative thermal ion mass spectrometry using a Thermo-Finnigan Triton instrument. Signals were detected using the electron multiplier (SEM) operating in pulse counting mode or faraday cups in static mode. Measured ratios were corrected for interferences from isobaric OsO_3^- molecules. Internal mass fractionation was corrected using a linear law and ^{192}Os/^{188}Os value of 3.08271 (Luck and Allègre, 1983). Monitoring of accuracy and long-term reproducibility for ^{187}Os/^{188}Os, by using the University of Maryland Osmium standard solution, yield 0.1141 ± 0.0001 (2σ, n = 30) on SEM and 0.11380 ± 0.00007 (2σ, n = 10) for measurements using faraday cups. For improved precision of ^{187}Os/^{188}Os values, we analyzed two times 50% of each sample aliquot on separate filaments. In Table 1 we report mean values and mean/√2 uncertainties.

All other HSE and sulfur were analyzed by sector-field inductively coupled plasma mass spectrometry using a Thermo-Fischer Element-XR instrument. The sample was introduced via conventional Scott-type glass spray chamber for Re, Ir, Pt, Au and S analyses and an Aridus membrane desolvation system was used for Ru, Rh, Pd, Ir and Pt. HSE signals were detected in low resolution mode with a SEM operating in pulse counting mode.

Cadmium, Tm, Yb, Lu, Hf, Ta, Os and Hg were analyzed to monitor isobaric interferences and potentially interfering oxide species. Oxide formation rates were <10% for the Scott-type spray chamber and <1% using the Aridus. Initial monitoring of Zr and Y revealed that the amount of elements which passes the cation resin is too low to produce measurable oxide interferences on Pd masses under the low oxide formation rate conditions during Aridus measurements. Lunar impact melt rocks are generally low in Zn and Cu and the interference potential of ZnAr and CuAr is low. Since Cd concentrations in lunar impact rocks are low (e.g. Ebihara et al., 1992) only minor interferences on Pd masses occurred. In addition, Pd concentrations were calculated from ^{105}Pd/^{108}Pd ratios, having the lowest interference potential. The internal precision of measured isotope ratios ranges from 0.1 to 1% ($2S_m$). Background-corrected element ratios were corrected for mass discrimination using IUPAC values by comparison with ratios in a HSE standard solution measured in the same sequence. Concentrations were generally determined by isotope dilution except for monoisotopic Rh and Au where a combined internal/external standardization technique using the ^{197}Au/^{193}Ir and ^{103}Rh/^{101}Ru ratios was applied (Fischer-Gödde et al., 2010).

Sulfur was analyzed in medium resolution mode to avoid molecular interferences from O_2, HS^- and Ni^{2+}. In order to monitor interferences from double charged ions, nickel and zinc were monitored. Based on monitoring and comparison of results obtained from ^{32}S/^{34}S and ^{32}S/^{33}S ratios the interferences from double charged ions were insignificant. The internal precision of measured isotope ratios was generally better than 0.5% ($2S_m$). Mass fractionation was determined and corrected by the comparison of the isotope ratios of a sulfur standard solution, which was prepared by using a K_2SO_4 reference material with known δ^{34}S (Wang et al., 2013).

3.4. Analytical blanks and uncertainties

Total analytical blanks (TAB) during the course of this study had an average of (±1σ): ^{187}Os/^{188}Os = 0.138 ± 0.028 and 1.5 ± 0.7 pg Re, 1.1 ± 0.3 pg Os, 1.6 ± 1.2 pg Ir, 1.0 ± 0.5 pg Ru, 12 ± 7 pg Pt, 1.9 ± 1.3 pg Rh, 21

Table 1
Highly siderophile element and sulfur concentration and osmium isotopic composition of Apollo 16 impact melt rocks.

	Weight [g]	Re [ng/g]	Re* [ng/g]	Os [ng/g]	Ir [ng/g]	Ru [ng/g]	Pt [ng/g]	Rh [ng/g]	Pd [ng/g]	Au [ng/g]	S [µg/g]	$^{187}Os/^{188}Os$ (±2σ)	$^{187}Re/^{188}Os$ (±2σ)
Intersertal impact melt rock (62295, 195)													
62295#1	0.09948	0.189	0.180	1.78	1.86	4.08	6.17	1.16	6.68	1.78	726	0.1338 ± 10	0.513 ± 38
62295#2	0.10081	0.156		1.45	1.49	3.01	4.69	0.884	4.54	1.37	1324	n.d.	0.519 ± 46
62295#3	0.09772	0.144	0.126	1.29	1.37	2.77	4.44	0.861	4.25	1.45	1532	0.1325 ± 14	0.538 ± 54
62295#4	0.09867	0.156	0.138	1.40	1.44	3.05	4.19	0.821	4.19	2.09	2888	0.1328 ± 13	0.539 ± 49
62295#5[MS]	0.00798	16.4	13.9	135	134	283	361	80.2	317	157	22952	0.1345 ± 2	0.589 ± 6
62295#6	0.08169	n.d.	0.112	1.10	1.16	2.40	3.15	0.475	3.07	1.16	2165	0.1340 ± 20	
62295#7	0.11716	0.194	0.200	2.04	2.05	4.21	5.47	0.919	5.49	2.00	576	0.1326 ± 8	0.458 ± 28
62295#8	0.10399	0.184	0.191	1.87	1.94	4.22	5.32	0.888	5.19	2.08	585	0.1341 ± 9	0.475 ± 35
62295#9	0.12661	0.165	0.196	2.17	2.19	4.04	5.12	0.803	4.39	1.93	558	0.1297 ± 7	0.367 ± 25
62295#10	0.07618	1.29	1.48	14.0	14.0	29.5	37.2	6.59	31.2	18.9	745	0.1356 ± 3	0.447 ± 6
62295#11[MS]	0.00533	17.5	17.3	170	169	347	436	78.1	375	147	3123	0.1342 ± 3	0.499 ± 7
Average[a]		0.540	0.524	4.84	4.87	10.1	13.2	2.48	11.9	5.38	1390	0.1341 ± 10	0.508 ± 39
Intergranular impact melt rock (65055, 54)													
65055#1	0.09959	0.620	0.640	7.30	7.05	11.9	15.0	1.96	10.8	2.61	1587	0.1287 ± 3	0.410 ± 9
65055#2	0.09861	0.322	0.336	3.88	3.71	6.20	7.51	1.03	3.01	1.27	1185	0.1283 ± 5	0.401 ± 18
65055#3	0.10941	0.403	0.415	4.73	4.47	7.54	9.34	1.28	4.14	1.98	1339	0.1287 ± 4	0.411 ± 13
65055#4	0.09132	0.951	0.551	6.46	6.09	10.3	12.7	1.83	5.71	1.98	775	0.1278 ± 3	0.709 ± 11
65055#5	0.11478	0.601	0.604	6.85	6.50	11.0	13.7	2.15	6.64	2.48	1977	0.1288 ± 3	0.423 ± 9
65055#6[MS]	0.00040	101	93.0	978	949	1707	2224	417	1566	n.d.	21736	0.1315 ± 5	0.499 ± 17
65055#7	0.09958	0.747	0.761	8.57	8.22	14.0	17.5	2.41	9.24	2.44	705	0.1291 ± 3	0.420 ± 8
65055#8	0.09363	0.433	0.442	5.16	4.91	8.21	10.6	1.47	4.47	1.49	1077	0.1279 ± 4	0.405 ± 14
65055#9	0.10442	0.334	0.334	3.82	3.67	6.19	7.63	1.02	3.30	1.03	700	0.1285 ± 5	0.421 ± 17
65055#10	0.10667	0.431	0.438	5.04	4.75	7.97	9.70	1.39	4.79	1.39	709	0.1283 ± 4	0.412 ± 13
65055#11	0.09798	0.850	0.858	9.44	9.00	15.5	19.6	2.99	11.0	3.72	677	0.1299 ± 2	0.434 ± 7
Average[a]		0.603	0.573	6.49	6.19	10.5	13.1	1.91	6.89	2.14	1096	0.1289 ± 6	0.464 ± 54
Hyaloophitic impact melt rock (61016, 512)													
61016#1	0.06936	0.086	0.069	0.633	0.634	1.32	1.58	0.255	1.48	0.707	b.d.l.	0.1368 ± 58	0.65 ± 15
61016#2	0.09024	0.079	0.033	0.291	0.282	0.574	0.794	0.113	0.628	0.276	b.d.l.	0.1381 ± 98	1.31 ± 26
61016#3	0.09535	0.036	0.031	0.278	0.269	0.578	0.706	0.090	0.514	0.249	b.d.l.	0.1374 ± 97	0.63 ± 26
61016#4	0.07470	0.026	0.016	0.142	0.124	0.280	0.573	0.044	0.707	0.199	b.d.l.	0.138 ± 24	0.87 ± 64
61016#5[LC]	0.12180	0.151	0.140	1.38	1.44	3.07	3.94	0.701	4.22	1.54	453	0.1340 ± 15	0.529 ± 40
61016#6	0.18863	0.054	0.049	0.443	0.437	0.921	1.23	0.190	1.08	1.01	622	0.1372 ± 31	0.592 ± 81
61016#7	0.16411	0.042	0.038	0.355	0.326	0.719	0.924	0.138	0.915	1.02	609	0.1365 ± 44	0.57 ± 12
61016#8[LC]	0.10161	0.155	0.141	3.30	2.30	3.12	4.27	0.641	3.42	2.62	12218	0.1115 ± 7	0.226 ± 20
Average[a,IM]		0.052	0.040	0.365	0.352	0.749	0.990	0.144	0.902	0.690	616	0.1371 ± 5	0.76 ± 23
Subophitic impact melt rock (64475, 110)													
64475#1	0.07757	1.89	1.97	17.4	18.6	40.5	51.0	9.16	45.7	26.2	1866	0.1385 ± 3	0.524 ± 5
64475#2	0.09087	1.72	1.86	16.5	17.6	35.9	46.3	7.69	37.8	24.3	1487	0.1381 ± 3	0.504 ± 5
64475#3	0.08256	1.72	1.76	15.6	16.8	36.5	46.5	7.78	40.7	23.1	938	0.1385 ± 3	0.534 ± 5
64475#4	0.07940	1.95	2.14	19.2	20.2	40.2	51.4	9.19	42.3	24.7	1511	0.1377 ± 3	0.491 ± 4

64475#5	0.07445	2.35	2.50	22.5	23.6	47.6	61.0	11.0	50.4	31.8	2465	0.1376 ± 3	0.505 ± 4
64475#6	0.07194	1.46	1.47	12.8	14.0	32.3	39.9	7.55	39.6	13.8	1471	0.1390 ± 3	0.548 ± 7
64475#7	0.06856	1.05	0.973	8.25	9.03	22.4	28.1	5.59	28.0	14.9	1020	0.1402 ± 4	0.616 ± 12
64475#8	0.07512	1.17	1.18	9.70	11.0	29.2	34.9	6.78	37.3	20.3	935	0.1417 ± 3	0.584 ± 9
64475#9	0.06977	0.706	0.711	5.98	6.61	16.4	20.3	4.06	24.0	7.27	1432	0.1406 ± 5	0.569 ± 16
64475#10	0.07157	1.50	1.52	13.4	14.4	30.9	39.7	7.34	38.3	20.7	1735	0.1387 ± 2	0.542 ± 7
64475#11[MS]	0.00088	109	106	980	1021	1804	2465	406	1770	580	b.d.l.	0.1363 ± 3	0.536 ± 8
64475#12[MS]	0.00059	17.4	18.5	159	170	396	519	98.4	545	222	20093	0.1397 ± 20	0.529 ± 72
64475#13[MS]	0.00415	126	130	1182	1216	2289	3018	570	2271	1303	6354	0.1371 ± 2	0.515 ± 1
64475#14[MS]	0.00522	31.7	32.3	282	304	667	842	159	732	358	5898	0.1389 ± 3	0.542 ± 5
64475#15[MS]	0.00355	7.77	6.87	53.1	60.2	185	216	49.5	264	111	2772	0.1446 ± 10	0.708 ± 36
Average[a]		2.60	2.68	23.8	25.2	52.8	67.6	12.4	58.6	31.3	1558	0.1382 ± 11	0.540 ± 28
Pokilitic impact melt rock (60335, 150)													
60335#1	0.10322	0.578	0.597	4.92	4.96	12.9	15.1	3.08	17.5	11.4	1189	0.1415 ± 4	0.568 ± 13
60335#2	0.10193	0.930	1.03	8.34	8.24	20.1	24.5	4.75	51.4	16.0	1163	0.1424 ± 3	0.538 ± 8
60335#3	0.10056	0.463	0.533	4.21	4.28	12.0	13.2	2.75	22.5	8.62	1687	0.1435 ± 5	0.530 ± 16
60335#4	0.10280	0.389	0.399	3.33	3.35	9.52	10.1	2.36	13.7	8.18	1541	0.1410 ± 6	0.564 ± 20
60335#5[MS]	0.00552	64.1	61.2	449	464	2077	1678	584	2855	1426	15425	0.1473 ± 3	0.691 ± 3
60335#6	0.11649	0.794	0.800	6.29	6.42	20.0	20.6	4.84	27.5	10.3	2014	0.1437 ± 3	0.609 ± 9
60335#7	0.08287	0.437	0.430	3.41	3.45	8.31	10.8	2.01	11.0	5.21	625	0.1434 ± 7	0.619 ± 24
60335#8	0.07463	0.747	0.770	6.66	6.58	14.5	18.4	3.42	17.2	11.2	511	0.1393 ± 4	0.541 ± 14
60335#9	0.07143	1.77	1.76	14.4	14.4	34.2	42.7	8.35	43.1	25.3	1109	0.1420 ± 3	0.594 ± 7
60335#10[MS]	0.00756	169	170	1450	1417	2219	3776	899	3057	2401	b.d.l.	0.1400 ± 2	0.5637 ± 6
60335#11[MS]	0.00670	125	129	1096	1093	2284	3113	807	3014	2219	5904	0.1402 ± 2	0.5484 ± 9
Average[a]		3.90	3.96	32.9	32.7	71.9	94.1	23.7	101	64.2	1419	0.1412 ± 14	0.576 ± 28

Re[*] calculated Re abundances according to Re/Os ratios required for the measured $^{187}Os/^{188}Os$ ratios starting from the solar system initial of 0.09531 at 4.558 Ga (Shirey and Walker, 1998). [MS]mineral separate, [LC]lithic clast, [a]mass-weighted average concentration data, and $^{187}Os/^{188}Os$ and $^{187}Re/^{188}Os$ (±2 σ_m). [IM]average values for 61016 excluding lithic clast aliquots, n.d. not detected, b.d.l. sulfur below detection limit.

± 7 pg Pd, 4.3 ± 5.6 pg Au, 1.1 ± 0.6 µg S (n = 11). For the full set of TAB values see Table 2 of the Electronic Supplement. All concentrations and isotope ratios were corrected for TAB contributions.

Absolute blank contributions depend on concentrations, but are generally <0.5% for Os, Ir and Ru, <3% Au and Rh, <5% Re, Pd and Pt and <20% for S. Slightly higher blank contributions occur in some subsamples of 62295 and metal separates with low weights (up to: 1.7% Os, Ir and Ru, 5% Au and Rh, 13% Re, Pd and Pt, 30% S). In sample 61016 the intermingling of impact melt with plagioclase glass lowers significantly the concentrations of all HSE and sulfur. Blank contributions are therefore higher when compared to other samples (0.3–15% Os, Ir and Ru, 7–43% Re, 1–36% Pt, Rh, Pd and Au, 1–17% S). The precision of concentration determinations is estimated based on blank contribution and precision of the measured isotope ratios (on average <0.3% for Os, <5% for Ir, Ru, Pt and Pd, and <10% for Re and S). Higher uncertainties result from lower concentrations in sample 61016 (<3% for Os and Ru, <20% for Ir and Pt, <37% for Re and Pd, and <30% for S). The precision of Rh and Au concentrations determined by standardization is estimated to be better than 10% and 15%, respectively.

4. RESULTS

4.1. Osmium isotopic composition

The osmium isotopic compositions, HSE and sulfur data for multiple aliquots of 5 lunar impact melt rocks are listed in Table 1. All but one sample are characterized by suprachondritic $^{187}Os/^{188}Os$ ratios similar to results reported for Apollo 16 impact melt rocks by Fischer- Gödde and Becker (2012) and Liu et al. (2015).

Rock and mineral separate aliquots of sample 62295 scatter over a range of $^{187}Os/^{188}Os$ and $^{187}Re/^{188}Os$ ratios without any isochronous relation (Fig. 1a). The $^{187}Os/^{188}Os$ average value of 0.1341 ± 10 (uncertainties are 2 r_m on the last digits shown) is identical within uncertainty to the value of 0.1343 ± 10 recently obtained by Liu et al. (2015) on a different split of the same sample. Aliquots of 64475 display a covariation of $^{187}Os/^{188}Os$ and $^{187}Re/^{188}Os$ ratios and a linear correlation with Os concentration (inset of Fig. 1b). The average $^{187}Os/^{188}Os$ of sample 65055 is chondritic (0.1289 ± 6). The isotopic composition of some aliquots tend towards slightly suprachondritic values, for instance in the sulfur-rich mineral separate which represents a minor fraction of the sample (inset of Fig. 1c). Nine rock aliquots and one mineral separate span a poorly defined errorchron of 2.45 ± 0.56 Ga. The initial $^{187}Os/^{188}Os$ ratio of 0.1114 ± 41 is chondritic within uncertainty (γOs = 1.0 ± 3.7). Most subsamples of sample 60335 define an apparent isochron with an age of 3.09 ± 0.42 Ga (Fig. 1d) and a slightly suprachondritic initial $^{187}Os/^{188}Os$ ratio of 0.1109 ± 44 (γOs = 4.8 ± 4.2). Two rock aliquots plot to lower Re/Os ratios and differ also in Ru/Pt ratios, indicative of a different component or process that fractionated those elements. Averaged rock and mineral separate values yield 0.1412 ± 14 the most radiogenic composition of a lunar impactite analyzed so far. Sample 61016 comprises of two lithologies, each with its own Re-Os systematics. The impact melt portion yields very low concentrations of Re and Os, therefore blank contributions and thus uncertainties are large (Fig. 1e). However, measured $^{187}Os/^{188}Os$ ratios are relatively uniform and fall into the range of suprachondritic samples (av. $^{187}Os/^{188}Os$ = 0.1371 ± 5). Two pieces of a grey lithic clast yield one order of magnitude higher concentrations, but contrasting $^{187}Os/^{188}Os$ ratios of 0.1340 ± 15 and 0.1115 ± 7, the latter value is strongly subchondritic, indicating a rather low time-integrated Re/Os in this aliquot.

Mineral separates display two orders of magnitude higher Re and Os concentrations and variable Os isotopic composition (Figs. 1 and 2). Irrespective of the average osmium isotopic composition of the sample, the highest Re/Os and $^{187}Os/^{188}Os$ ratios were obtained from sulfur rich mineral separates which also display more fractionated HSE pattern than the less radiogenic mineral separates (Fig. 3).

In order to detect possible disturbances in the Re/Os ratios, Re^* abundances were calculated from the measured Os isotopic composition of the sample assuming its evolution from an initial solar system $^{187}Os/^{188}Os$ value of 0.09531 at 4.558 Ga (Shirey and Walker, 1998) with a λ of $1.666 * 10^{-11}$ a^{-1} (Smoliar et al., 1996). Relative deviations range from −18.7% to 12.3% for 62295, −9.4% to 11.7% for 64475, −4.2% to 8.1% for 65055, and −15.1% to 4.6% for 60335.

4.2. Highly siderophile element and sulfur composition

The average HSE concentrations of four analyzed rocks vary over two orders of magnitude from 0.01 to 0.4 times CI chondrite. The highest absolute concentrations were detected in samples 60335 and 64475, slightly above HSE concentrations in impact melt rocks reported by Fischer- Gödde and Becker (2012). The sulfur concentrations are less variable and range from 0.02 to 0.03 times CI chondrite. The subsample aliquots of the lunar impactites generally display straight correlations when displayed in Ir vs. HSE diagrams (Fig. 2). Rock subsample aliquots of 62295 and 64475 display slightly curved trends towards higher concentrations, except for Os/Ir (Fig. 2a and b). Similar curved trends were observed in impact rocks 60315 and 67935 by Fischer-Gödde and Becker (2012). Palladium vs. Ir diagrams usually display somewhat larger scatter which was observed in previous studies as well and does not reflect analytical scatter (Fischer-Gödde and Becker, 2012; Sharp et al., 2014; Liu et al., 2015). No correlation was observed between sulfur and the HSE, indicating that both are not controlled by the same phases.

Mineral separates vary in absolute and relative concentrations of HSE and S. Mineral separates with low sulfur contents display the highest HSE concentrations and at the same time the least fractionated patterns when normalized to CI chondrite (Fig. 3). On the other hand, HSE patterns become significantly more fractionated with increasing sulfur content. For example, the strongly magnetic subsample 60335#10 contains 1.4 µg/g Ir with Au/

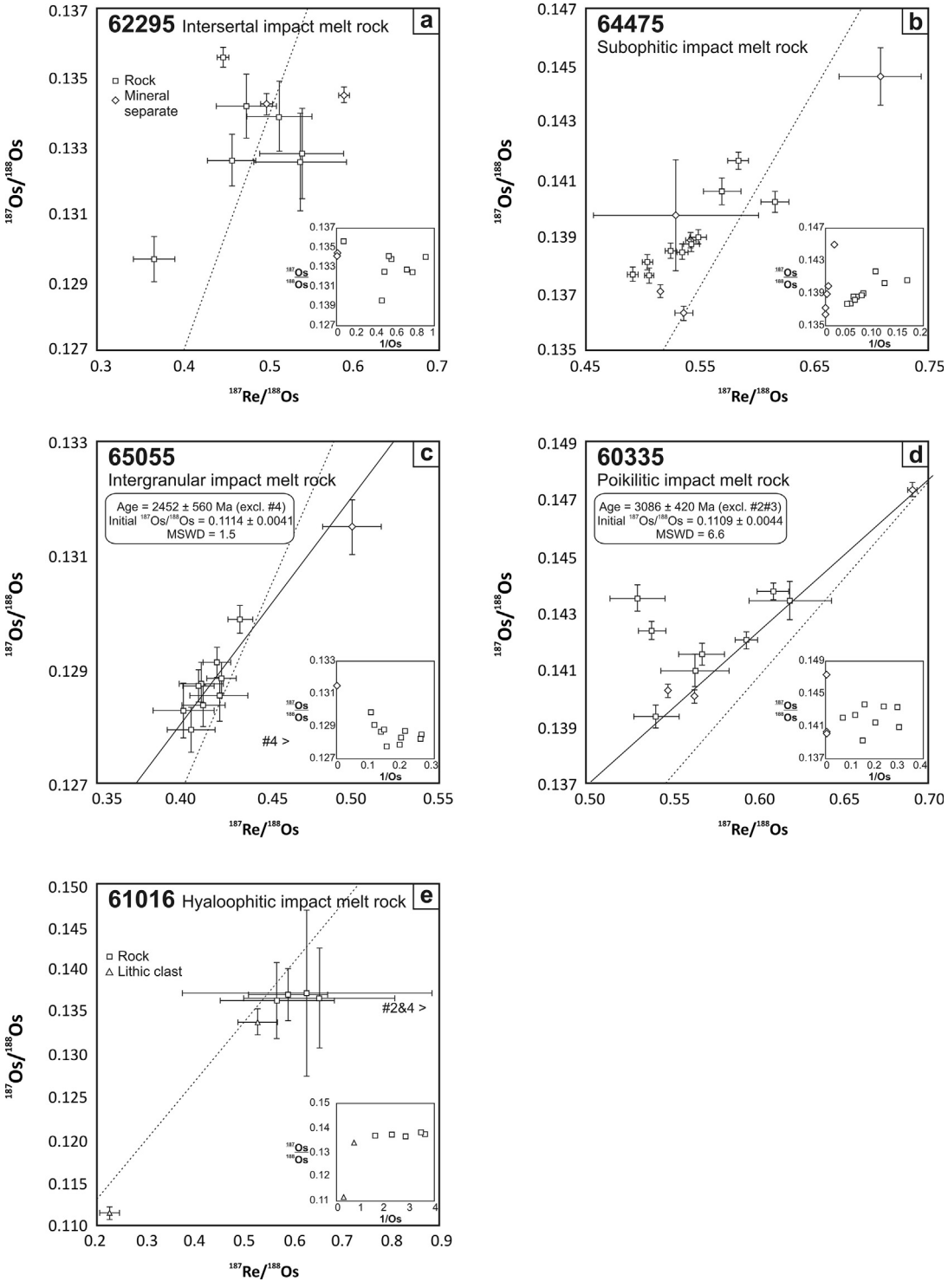

Fig. 1. Osmium isotopic composition in subsamples of Apollo 16 impact rocks (uncertainties are 2σ). Insets are $^{187}Os/^{188}Os$ vs. 1/Os for the subsamples of the respective rock. (A) 4.0 Ga reference line with a chondritic initial $^{187}Os/^{188}Os$ is shown for comparison.

Ir = 1.7. In contrast, the magnetic and weakly magnetic mineral separates of the latter sample contain 0.5–1 µg/g Ir and display increasing Au/Ir ratios from 2 to 3, increasing enrichment of Re over Os and a characteristic enrichment of Ru over Pt (Fig. 3c).

4.3. Determination of element ratios from multiple aliquots

Two different methods were employed to obtain bulk HSE/Ir ratios from multiple aliquots which were measured for each sample (Table 2). In the first approach, linear

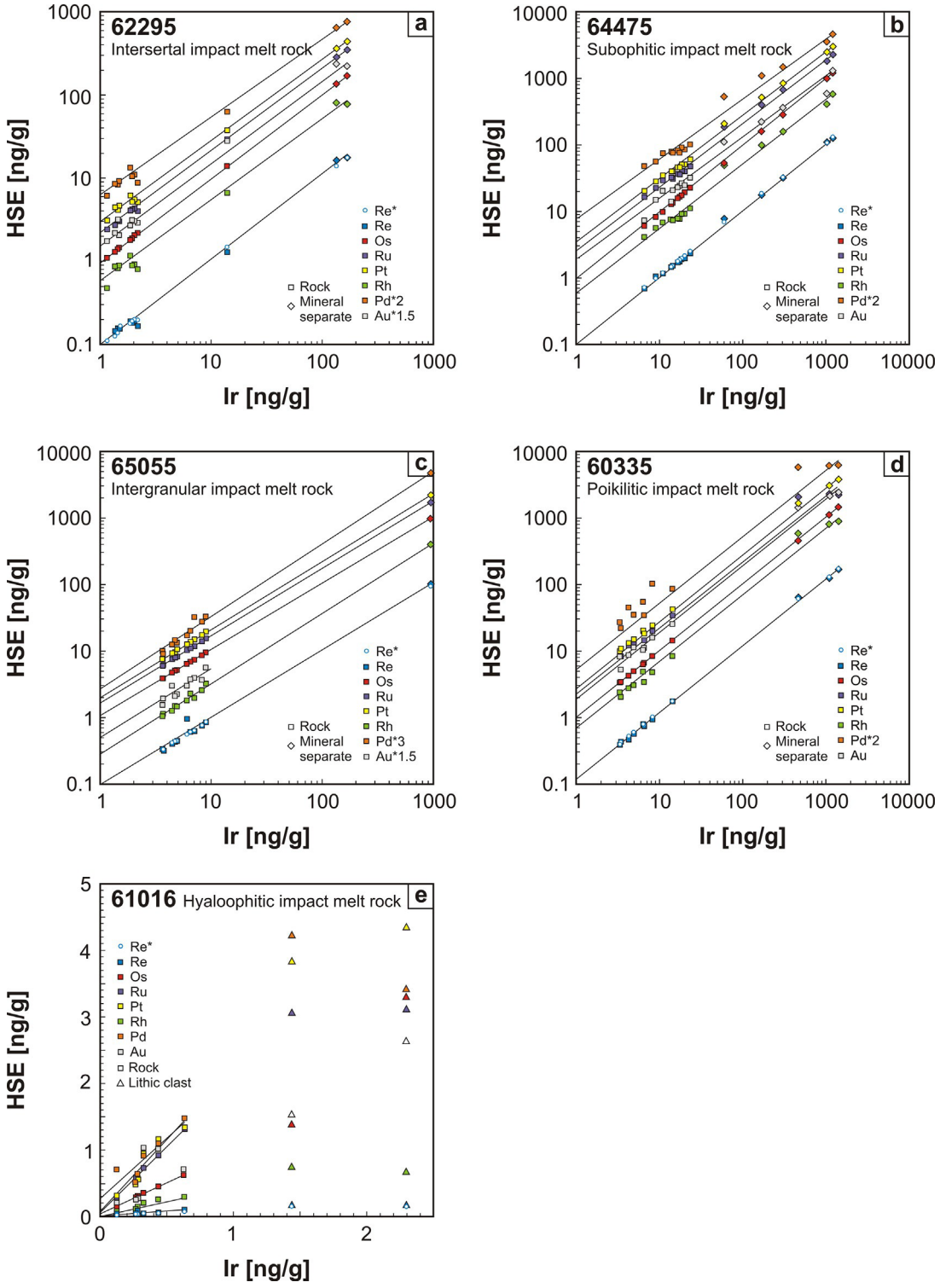

Fig. 2. Highly siderophile element concentrations in subsamples of Apollo 16 impact rocks, mineral separates and lithic clasts. (a–d) logarithmic scale due to high concentrations in mineral separates. Uncertainties are usually smaller than the size of the symbols. Linear regression calculations are shown for illustration. Intercept and slope values are given in Table 2.

regressions of HSE vs. Ir were calculated (Fig. 2), including rock aliquots and mineral separates using the Isoplot 3.75 software (Ludwig, 2012). The intercept values of these regression calculations are zero within uncertainty or close to zero for samples 62295, 60335 and the impact melt rock portion of 61016. Significant deviations from zero occur for

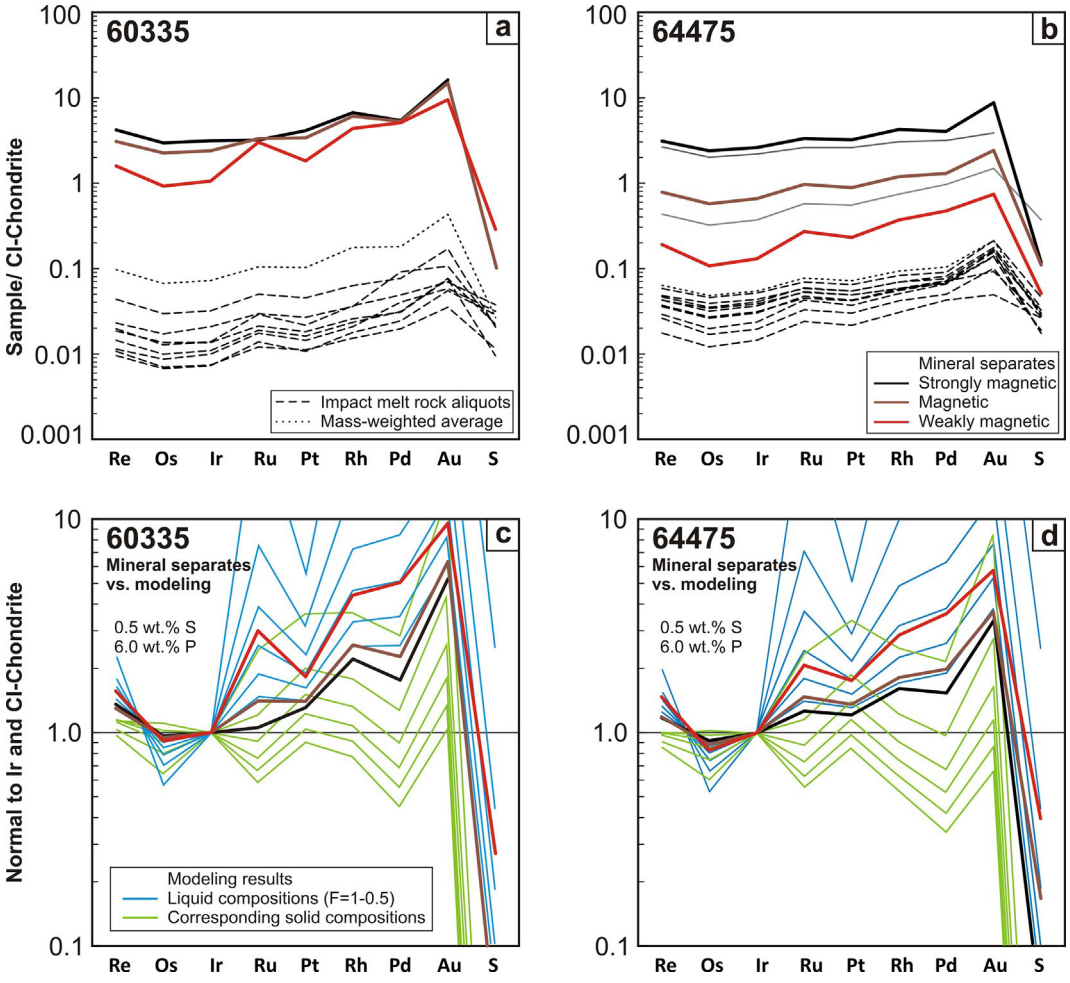

Fig. 3. (a and b) CI chondrite normalized HSE and S pattern for individual aliquots of sample 60335 and 64475. (c and d) Measured HSE/Ir ratios and S/Ir ratios normalized to CI chondrite for individual mineral separate aliquots together with the results of crystallization modeling considering the effects of light elements (see text for details). Elements are displayed in the order of decreasing 50% condensation temperature from a gas of solar composition. CI chondrite HSE data of Fischer-Gödde et al. (2010) and sulfur data of Dreibus et al. (1995) were used for normalization.

Os, Ru, Pt, Rh and Pd in 65055 and 64475. In the second approach HSE/Ir ratios were calculated from weighted averages of concentration determinations (Table 1). The latter approach better accounts for the mass balance and the measured element budget of the samples. The results obtained by the different methods are generally in good agreement for Re, Os, Ru and Pt, and within the 95% confidence interval for Rh, Pd and Au. However, it is noteworthy that the values obtained from weighted averages of the more fractionated samples, although within uncertainty of the regression calculations, are usually higher for Ru, Pt, Rh, Pd and Au (Fig. 2 of the Electronic Supplement). Another notable observation is that Pd/Ir in 65055 yields either a sub- or suprachondritic value, depending on the calculation method applied to the same data.

Samples 62295, 60335 and 64475 display subchondritic Os/Ir and increasingly fractionated HSE/Ir ratios from Ru towards Au and characteristic enrichments of normalized Re over Os and Ru over Pt (Fig. 4a), similar to Apollo 16 samples analyzed by Fischer-Gödde and Becker (2012) and Liu et al. (2015). Sulfur/Ir ratios are subchondritic in 60335 and 64475, but suprachondritic in 62,295. In contrast, the intergranular impact melt rock 65055 displays a normalized HSE + S/Ir pattern with only minor deviations from CI chondrite ratios, similar to three basaltic impact melt rocks samples from Apollo 16 analyzed by Liu et al. (2015). Notable are the slight enrichments of normalized Re over Os and Ru over Pt, in this sample, although less pronounced than in the strongly fractionated samples (Fig. 4a). In contrast to the neighboring Rh and Au, Pd is slightly depleted, a pattern similar to granulitic impactites reported by Fischer-Gödde and Becker (2012). The impact melt portion of sample 61016 yielded HSE concentrations 1–2 orders of magnitude above pristine lunar crustal rocks (e.g. Day et al., 2010 and references therein). Its HSE/Ir ratios are in the range of the non-chondritic samples, but S/Ir is much higher (Fig. 4a). The lithic clast attached to 61016 yields on average chondritic refractory HSE/Ir ratios, whereas Rh/Ir, Pd/Ir, Au/Ir and S/Ir ratios are increasingly suprachondritic.

Table 2
Intercepts and slopes for linear regression calculations and element ratios obtained from weighted averages of concentration values.

Sample	62295	60335	61016	65055	64475
Intercept values [ng/g]					
Re	−0.036 ± 70	0.01 ± 10	0.019 ± 58	−0.03 ± 24	−0.011 ± 68
Re^*	−0.014 ± 12	0.013 ± 31	0.0038 ± 83	−0.023 ± 18	0.007 ± 19
Os	−0.055 ± 27	−0.062 ± 94	0.030 ± 28	0.058 ± 97	−0.43 ± 28
Ru	−0.09 ± 22	3.3 ± 2.8	0.032 ± 62	−0.39 ± 18	3.7 ± 3.2
Pt	0.27 ± 51	1.2 ± 1.1	0.18 ± 18	−0.87 ± 46	4.1 ± 2.9
Rh	0.00 ± 23	−0.27 ± 89	0.016 ± 18	−0.42 ± 27	0.8 ± 1.2
Pd	0.77 ± 77	7.2 ± 7.3	0.23 ± 28	−2.9 ± 2.0	9.2 ± 5.5
Au	−0.10 ± 41	−0.5 ± 2.5	−0.04 ± 57	−0.27 ± 67	3.9 ± 4.4
Slope					
Re/Ir	0.108 ± 11	0.1165 ± 38	0.09 ± 15	0.102 ± 39	0.1029 ± 32
Re^*/Ir	0.1043 ± 23	0.1204 ± 30	0.103 ± 22	0.0965 ± 30	0.1056 ± 11
Os/Ir	1.0036 ± 55	1.0056 ± 89	0.957 ± 74	1.040 ± 16	0.958 ± 17
Ru/Ir	2.100 ± 50	2.07 ± 29	2.05 ± 17	1.760 ± 30	1.96 ± 20
Pt/Ir	2.642 ± 89	2.835 ± 96	2.33 ± 47	2.260 ± 76	2.50 ± 17
Rh/Ir	0.48 ± 12	0.68 ± 16	0.448 ± 56	0.377 ± 51	0.464 ± 73
Pd/Ir	2.25 ± 14	2.61 ± 81	1.93 ± 75	1.57 ± 32	1.90 ± 29
Au/Ir	1.02 ± 22	1.93 ± 44	1.4 ± 2.0	0.38 ± 13	0.93 ± 27
Average					
Re/Ir	0.1008 ± 81	0.1195 ± 29	0.148 ± 42	0.0975 ± 27	0.1033 ± 14
Re^*/Ir	0.1075 ± 15	0.1213 ± 7	0.1139 ± 93	0.0925 ± 5	0.1062 ± 4
Os/Ir	0.993 ± 14	1.007 ± 54	1.037 ± 84	1.0482 ± 52	0.943 ± 36
Ru/Ir	2.079 ± 31	2.202 ± 13	2.13 ± 18	1.698 ± 10	2.960 ± 93
Pt/Ir	2.70 ± 11	2.951 ± 34	2.45 ± 41	2.119 ± 29	2.721 ± 22
Rh/Ir	0.508 ± 51	0.725 ± 73	0.409 ± 52	0.309 ± 31	0.492 ± 49
Pd/Ir	2.43 ± 12	3.096 ± 50	2.56 ± 72	1.114 ± 51	2.325 ± 25
Au/Ir	1.10 ± 17	1.97 ± 30	1.96 ± 33	0.346 ± 52	1.24 ± 18
$S/Ir^* 10^{-3}$	285 ± 42	43.4 ± 6.0	1749 ± 260	177 ± 25	61.8 ± 8.2

Uncertainties for values of intercept and slope of regression calculations were calculated at 95% confidence interval and refer to the last decimal places. Average element ratios are calculated from mass-weighted average concentrations given in Table 1. Uncertainties for HSE/Ir and S/Ir ratios are error propagated 2σ uncertainties of concentration determinations for each element, weighted for each aliquot. Only the aliquots of the impact melt portion of sample 61016 were considered for regression calculation and averages.

5. DISCUSSION

5.1. Behavior of highly siderophile elements during the formation of ancient lunar melt rocks

In order to obtain precise element ratios from gram-size sample volumes of lunar impactites, multiple aliquots were analyzed and a regression approach was used. Variable concentrations due to incomplete mechanical mixing of low-HSE target and the high-HSE impactor should produce a strong correlation between elements of impactor origin (Palme, 1980). It is believed, that the slope of regression lines determines the element ratios of the impactor and the deviation of the regression y-intercept from zero represents the indigenous contribution to the HSE budget. Recent publications employed this method in combination with precise isotope dilution measurement of HSE (Puchtel et al., 2008; Fischer-Gödde and Becker, 2012; Sharp et al., 2014; Liu et al., 2015). However, interpretation of the obtained HSE ratios is sometimes hampered by devia- tions from true linearity or non-zero intercepts of regression lines. Before HSE ratios are used to constrain putative impactor compositions or assigning specific samples to basin forming events, it is necessary to rule out other processes which might have fractionated the HSE during impact and post-impact processes. In the following sections we will mainly discuss five questions relevant to Apollo 16 impact melt rocks with implications for lunar impact processes in general.

(1) Are HSE carrier phases in Apollo 16 impact melt rocks remnants of specific impactors or did they crystallize from liquid metal droplets after equilibration with homogenized impact melts (Section 5.1.1.)?
(2) What is the origin of the moderately volatile siderophile elements sulfur and phosphorous, and were the HSE fractionated by impact volatilization (Section 5.1.2.)?
(3) How do light elements influence solid metal-liquid metal fractionations during crystallization of impact melts (Section 5.1.3.)?
(4) Do HSE ratios reflect the composition of late accreted material or fractional crystallization and segregation of metal within the impact melt sheet (Section 5.1.4.)?
(5) Are HSE ratios obtained from a limited number of small aliquots representative for the entire sample and what is the most reliable method to obtain HSE ratios of the bulk rock (Section 5.1.5.)?

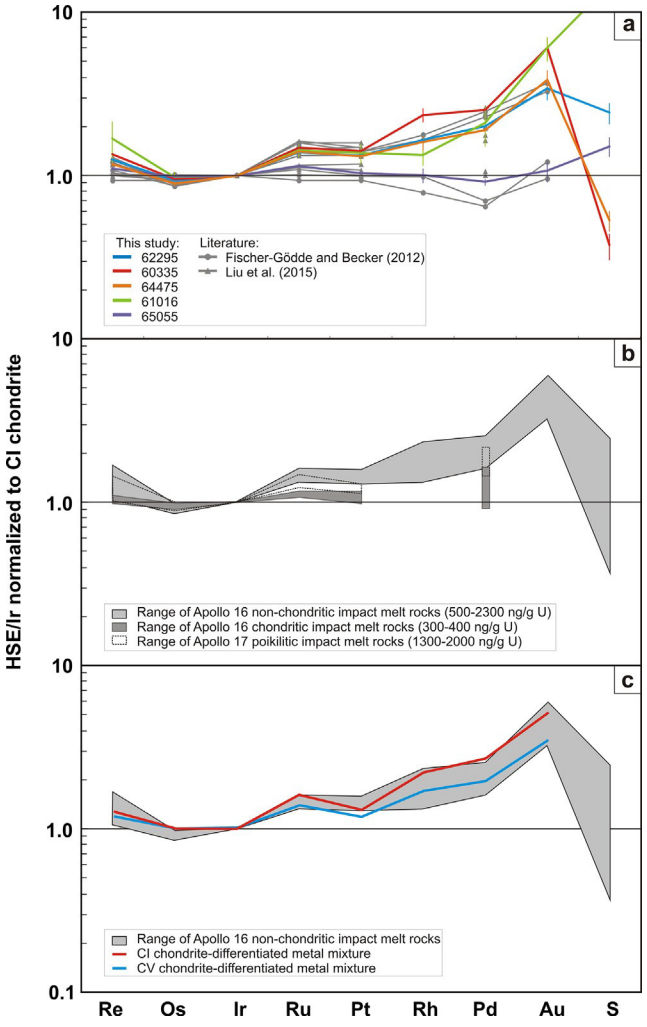

Fig. 4. HSE/Ir and S/Ir ratios of bulk impactites normalized to CI chondrite values (CI values and arrangement of elements as in Fig. 3). All literature data were recalculated to weighted average values (see text for explanation). (a) Apollo 16 impact rocks including impact melt rocks (Fischer-Gödde and Becker, 2012; Liu et al., 2015; this study) and granulitic and polymict impact breccias (Fischer-Gödde and Becker, 2012). Uncertainties are error propagated 2σ uncertainties of concentration measurements as listed in Table 2. (b) Comparison between the range of Apollo 16 non-chondritic and KREEP-rich (n = 11) and chondritic (n = 4) impact melt rocks and the range of Apollo 17 poikilitic impact melt rocks (n = 7; Puchtel et al., 2008; Sharp et al., 2014). (c) Calculated mixture between 85% of chondritic compositions (Fischer-Gödde et al., 2010) and 15% of differentiated metal of a main group pallasite (Danielson et al., 2009).

5.1.1. Influence of solid metal-liquid metal partitioning on HSE fractionation in lunar impact melt rocks

Available isotope dilution data on Apollo 16 impactites shows differences in absolute and relative HSE abundances between both, different samples from the same landing site and within aliquots of individual samples (Fischer-Gödde and Becker, 2012; Liu et al., 2015, this study). In addition, stepwise LA-ICP-MS analyzes of rim and core of metal globules from different landing sites yielded highly variable siderophile element ratios (James et al., 2007; Norman and Roberts, 2013; Liu et al., 2015) indicating small-scale fractionation processes. Recent experimental work has indicated that the partitioning of HSE in the Fe-Ni system is strongly dependent on the concentration of light elements (Corrigan et al., 2009; Chabot et al., 2014 and references therein). In order to better constrain this influence during impactite formation, their abundance and partitioning behavior needs to be evaluated before interpreting observed distributions of HSE.

In many ancient lunar impactites Fe-Ni metal, phosphides and sulfides are common phases, whereas carbides are scarce (Gooley et al., 1973; McKay et al., 1973; Vaniman and Papike, 1980; Hunter and Taylor, 1981, and references therein). These phases form intergrowths which are usually subrounded when enclosed in mesostasis, or follow the silicate grain boundaries in subophitic and holocrystalline samples (e.g. Gooley et al., 1973; McKay et al., 1973; Misra and Taylor, 1975). Such textural characteristics argue against physical mixing of solid meteoritic metal into impact rocks, but imply late crystallization after the majority of the silicates (e.g. Misra and Taylor, 1975; Norman and Nemchin, 2014). The excess abundances of

W, P and also sometime so Ge and Co, which are interpreted to be of indigenous lunar origin, argue strongly for chemical equilibration between liquid metal droplets and silicate impact melt (Wlotzka et al., 1972; McKay et al., 1973; Misra and Taylor, 1975; Palme et al., 1982; Norman and Roberts, 2013; Norman and Nemchin, 2014). The ubiquitous abundance of schreibersite and troilite in concentric or eutectic texture with the Fe-Ni metal indicates the presence of sulfur and phosphorous in the liquid metal in the range of several weight percent.

During the formation of impact melt rocks, light elements like sulfur and phosphorous act in two important ways. Firstly, they lower the liquidus temperatures in the Fe-Ni system, which leads to the melting of all HSE carrier phases even when some refractory silicate minerals may survive. Secondly, during cooling and crystallization, solid metal/liquid metal partitioning of the HSE is strongly affected by the presence of different light elements (Chabot et al., 2014 and references therein). Our data show that absolute and relative HSE compositions of opaque phases are related to their sulfur (and likely also phosphorous) content. Mineral separates displaying the lowest sulfur contents generally have the highest absolute concentrations, but the least fractionated HSE pattern, whereas separates with lower concentrations, but more fractionated HSE patterns are generally accompanied by higher sulfur contents (Table 1; Fig. 3). Together with the above textural observations we interpret this as a strong argument for sub-centimeter-scale fractional crystallization of solid Fe-Ni metal from Fe-Ni-P-S liquid droplets in silicate impact melt during cooling as suggested by James et al. (2007) and Fischer-Gödde and Becker (2012).

5.1.2. Origin and behavior of sulfur and phosphorous in lunar impactites

The HSE are undoubtedly meteoritic, whereas the moderately siderophile elements S and P are most likely of mixed origin. Concentration data on impactites range from 50 to 2000 μg/g sulfur and 40 to 3000 μg/g phosphorus, whereas carbon is low (10–150 μg/g, Haskin and Warren, 1991; see also compilation of literature data in Table 1 of the Electronic Supplement). Available concentration data for monomict highland rocks indicate 50 to 950 μg/g sulfur, 40 to 3000 μg/g phosphorus and <15 μg/g carbon (Haskin and Warren, 1991). The concentrations of these elements are usually lower in ferroan anorthosites than in magnesium suite rocks. A high P concentration in KREEP testifies to its incompatible behavior during mantle crystallization, but no data are available for S and C .

Comparison of the absolute concentration of light elements in target and putative impactor compositions reveals large differences when compared to HSE. The overall impactor/target ratio decreases from highly siderophile (10^5) to moderately siderophile sulfur (10^2) and phosphorus (10^1–10^0), assuming CI-chondritic impactor compositions and pristine lunar highland crust. Therefore, in impact melt containing approximately 1% of a CI-chondritic impactor component, almost half of the sulfur and virtually more than 90% of the phosphorous would be of lunar origin. Assimilation of large amounts of KREEP component or consideration of impactors different from CI chondrites would change further the light element mass balance of the impact melt.

A lunar origin of a significant fraction of P and S is supported further by thermal reduction of phosphate to phosphide, observed in laser induced heating experiments on basalt-chondrite mixtures under an oxygen free atmosphere (Yakovlev et al., 2006). Major proportions of iron and phosphorous were thermally reduced to its metallic state during experiments, whereas sulfur mainly occurs as S^{2-} in accordance with the frequent observation of metal, schreibersite and troilite in lunar impact melt rocks (e.g. Gooley et al., 1973; McKay et al., 1973; Misra and Taylor, 1975; Hunter and Taylor, 1981). The latter experiments have also demonstrated that iron and more volatile elements like S and P are present in the vapor phase under temperature conditions of impact melt formation (Yakovlev et al., 2006). A recent LA-ICP-MS study of vapor deposited metal particles in vesicles of a lunar impact melt rock revealed measurable concentrations for siderophiles more volatile than Fe, however, bulk loss of siderophiles could not be detected (James et al., 2007). Our combined HSE and S data provide further constraints against volatility-controlled losses during impact, for two reasons. Firstly, in accordance with previous studies, in general concentrations of moderately volatile elements Pd and Au are higher than some of the more refractory HSE's and good correlations between moderately volatile and refractory HSE's are observed in aliquots of the same sample (see also discussion in Puchtel et al., 2008 and Fischer-Gödde and Becker, 2012). Secondly, we do not observe a correlation with more volatile sulfur. In contrast, we observe the highest Au/Ir ratios in mineral separates (Fig. 3), which, according to phase relations in the Fe-Ni-P-S system were interpreted to crystallize late, encompassing the highest risk to undergo volatile loss.

Both P and S are moderately siderophile at low pressure and prefer the liquid metal phase (Schmitt et al., 1989; Rose-Weston et al., 2009; Boujibar et al., 2014). However, while phosphorus partitions strongly into the metallic liquid, especially if it is reduced to its metallic state (Yakovlev et al., 2006), the solubility of sulfur in liquid metal is significantly reduced under low oxygen fugacity conditions, in particular if the liquid metal contains considerable amounts of P (Boujibar et al., 2014 and references therein). These boundary conditions are consistent with measured P/S ratios of ~~3~~–4 in separated metal spherules (Palme et al., 1982). The concentration of metallic spherules in Apollo 16 impact melt rocks is variable, but usually below 2 vol.% (Hunter and Taylor, 1981) and indicates the amount of immiscible metallic liquid during final cooling. Assuming average concentrations of 500 μg/g in the bulk melt for both sulfur and phosphorous (Table 1 of the Electronic Supplement), at low oxygen fugacity (<IW) and low pressure conditions, 0.25–2.5 wt.% S ($D_S^{met/sil}$ 5–50) and 2.5–7.5 wt.% P ($D_P^{met/sil}$ 50–150) can be estimated in the metallic liquid (Schmitt et al., 1989; Rose-Weston et al., 2009; Boujibar et al., 2014). These estimations are in agreement with the observed amount of schreibersite and troilite (Misra and Taylor, 1975; Hunter and Taylor,

1981) and our new determinations of sulfur concentrations in mineral separates (Table 1). Light element concentrations in the range of several wt.% will strongly affect the partition behavior of HSE during crystallization and the effect of phosphorus should be taken into account, given the ubiquitous presence of schreibersite (Misra and Taylor, 1975; Hunter and Taylor, 1981).

5.1.3. Modeling of solid metal-liquid metal fractionation in the Fe-Ni-P-S system

In order to test whether average whole rock HSE compositions of lunar impact melt rocks are representative of the melts they crystallized from or if large-scale fractional crystallization and segregation of metal may have affected the HSE composition of the impactites, we decided to model HSE partitioning between solid and liquid metal during crystallization of immiscible Fe-Ni-P-S liquids. The recent parameterization for solid metal-liquid metal partition coefficients in the Fe-Ni-P-S-C system of Chabot et al. (2014) compiles experimental work at conditions of 1 atm and 1050–1500 °C, applicable for post-shock crystallization of impact melt rocks. The parameterization accounts for the combined influence of sulfur and phosphorus on HSE partition coefficients. We used a constant $D^{sm/lm}$ (solid metal-liquid metal partition coefficient) value of 0.01 for S (Chabot et al., 2009) and calculated $D^{sm/lm}$ values for P, which depend on S concentrations in the liquid metal and range from 0.1 to 0.2 (Chabot et al., 2014). Since both elements are incompatible in solid metal (Corrigan et al., 2009; Chabot et al., 2009), their concentrations increase in the liquid metal phase, as crystallization proceeds. To account for changes in the composition of liquid metal, we adjusted the $D_{HSE}^{sm/lm}$ values for each 1% crystallization step according to changes of S and P concentrations in the liquid metal. Unmixing of two metallic liquid compositions, one S-rich and the other P-rich, may occur at advanced stages of crystallization, but depends on initial concentrations of these elements in the metallic liquid and oxygen fugacity (Chabot and Drake, 2000). Regarding the S and P concentrations, estimated to account for compositional trends in lunar impactites, the residual metallic liquid would reach the two liquids field late (i.e. after more than 60% crystallization). At this stage, most HSE have already been incorporated in solid metal and liquid immiscibility would not affect the model calculation, except for minor effects on Pd and Au.

Mineral separates display the largest spread in absolute concentrations and element ratios and are therefore interpreted to reflect different compositional stages of liquid metal solidification. A conspicuous feature is the correlation between increasing Ru/Pt and the overall fractionation and steepness of HSE patterns, which is also related to changes in sulfur contents (Fig. 3a and b). Among the light elements, sulfur concentration has a strong effect on solid metal-liquid metal partition coefficients ($D^{sm/lm}$) for all HSE, but does not strongly alter the relative partitioning of Ru and Pt. In contrast, phosphorous lowers the solid metal-liquid metal partition coefficient for Ru and concentrations higher than 2.5 wt.% in liquid metal yield $D_{Ru} < D_{Pt}$, which, upon crystallization, leads to increasing Ru concentrations in the residual liquid when compared to Pt. Carbon concentrations in impact melt rocks are generally low and minor amounts do not significantly alter the D values (e.g. contribution of 0.25 wt.% C would change $D^{sm/lm}$ by less than 1.5%). Its influence on solid metal-liquid metal partition of HSE was therefore ignored for the current modeling. For the purpose of fitting the modeling results to data from impactites and possible initial liquid metal compositions we decided to model HSE/Ir and S/Ir ratios instead of concentrations, because absolute HSE abundances in the liquid metal depend on the fraction of impactor material in the impactites and the metal content and are therefore not diagnostic for specific impactor compositions. Furthermore, the HSE and S concentrations of mineral separates might be diluted by incomplete separation from silicate phases.

5.1.4. Modeling HSE fractionation between solid metal and liquid metal during impact melt crystallization

With the objective of discrimination between realistic and unrealistic scenarios, we tested different starting HSE compositions and variable light element contents, in order to access which composition reproduce best the element ratios observed in mineral separates of different magnetic susceptibility (i.e. composition). Using the relative HSE abundances derived from weighted averages of all aliquots of impact melt rocks 60335 and 64475 as a starting composition of metal melt droplets together with reasonable abundances of sulfur and phosphorous (0.25–2.5 wt.% S and 2.5–7.5 wt.% P, see Section 5.1.2.) yields increasingly fractionated liquid and solid metal compositions during crystallization modeling. Hereby, the magnetic and weakly magnetic mineral separates are satisfactorily explained by light element contents of 0.5 wt.% sulfur and 6 wt.% phosphorus (Fig. 3c and d). In detail, the HSE compositions of magnetic mineral separates closely resemble the starting composition of our modeling (Fig. 3a and b). This interpreted as signature of solidified droplets of initial metal melt. The latter seems to be the most common HSE carrier phase, even in aliquots with low absolute HSE content, which is supported further by their osmium isotopic composition which is almost identical of the bulk samples. The HSE composition of the weakly magnetic fraction fits a calculated residual metallic liquid composition after fractional crystallization of roughly 20% Fe-Ni metal. This interpretation is consistent with the higher sulfur content observed in these fractions (Fig. 3a and b), which is indicative of higher concentrations in the metal as well as additional FeS from late stage S-rich metallic liquid. In contrast, the strongly magnetic fraction displays the highest absolute HSE content, but the least fractionated pattern, consistent with accumulation of early solid metal (Fig. 3c and d). Calculated solid metal compositions display some of the features observed in the strongly magnetic fraction like low Ru/Pt and Pd/Au ratios (Fig. 3c and d) which stem from lower $D^{sm/lm}$ values of Ru and Pd during early metal solidification.

Some compositional features observed in the mineral separate data sets cannot be explained by calculated solid metal-liquid metal partitioning, but reflect troilite and

schreibersite formation near the eutectic. Slight deviations in Pd and Au abundances of measured mineral fractions from calculated liquid compositions are due to the incompatibility of these elements in solid metal at the beginning of the crystallization process (Chabot et al., 2014). Therefore, these elements become enriched in the residual melt, which after separation of P-rich and S-rich melt phases, form schreibersite and troilite. From textural observations (e.g. Gooley et al., 1973; Misra and Taylor, 1975) and phase relations (e.g. Chabot and Drake, 2000) it is very likely that schreibersite is formed first and then troilite. Both occur together with late crystallized metal and thus are included in weakly magnetic mineral separates. Admixture of these phases can influence Pd and Au concentrations. Rhenium abundances of the weakly magnetic fraction higher than calculated are explained similarly by attached schreibersite. A detailed investigation of metal-sulfide-phosphide intergrowths in iron meteorites by Shen et al. (1996) reveals that schreibersite in equilibrium with metal contains small but significant amounts of Re and Os, with high Re/Os and $^{187}Os/^{188}Os$ much more radiogenic than in the metal. This is consistent with the measured isotopic composition of strongly magnetic (pure metal) and weakly magnetic mineral separates (attached schreibersite-troilite component) in impact melt rocks (Fig. 1). In principle, the observed Re/Os fractionation and the measured differences between mineral separates of different composition can place a time constraint on the partitioning process (see discussion in Section 5.2.1.).

Like many Apollo 16 impact melt rocks, the studied samples share HSE compositional and osmium isotopic characteristics with members of the IVA iron meteorite group (Fischer-Gödde and Becker, 2012; Liu et al., 2015). However, apart from the overall similarities some characteristic element ratios like Ru/Pt are different from IVA iron compositions. In accordance with this observation, solid metal-liquid metal partitioning models that use a starting composition like the fractionated IVA iron meteorite Bushman Land yield residual metallic liquids which are too fractionated and fail to produce the Ru/Pt and Pd/Au ratios observed in the weakly magnetic and sulfur rich mineral separates. It follows that the fractionated metal in the Apollo 16 impactites most likely was not derived from the IVA core. IVA iron compositions less fractionated than Bushman Land were not considered here because their $^{187}Os/^{188}Os$ ratios are lower than some of the sample studied here.

Fractionated HSE patterns in impact melt rocks may also be generated if crystallizing solid metal is gravitationally removed from an initially unfractionated primitive metallic melt composition which is dispersed in the impact melt. Recent models for igneous differentiation of large (basin-sized) impact melt pools (e.g. Vaughan et al., 2013) raise the question, if magmatic accumulation of metal may have occurred, which produced the variability in absolute and relative HSE abundances observed in lunar impact melt rocks. To test this hypothesis, we used metal compositions that show CI and EH chondrite-like HSE abundance patterns. Light element contents in the metallic melt were adjusted to impact melt compositions as discussed in Section 5.1.1. (i.e. low in sulfur but relatively rich in phosphorus). Although the overall fractionated HSE pattern of whole rocks and mineral separates could then be explained, the high degree of fractional crystallization of solid metal makes such a process unlikely. In detail, the magnetic fraction and the whole rock composition would be matched after roughly 30–40% of solid metal crystallization, whereas the weakly magnetic fraction requires at least 60–80% crystallization. EH chondrite compositions provide a better match for the high Au/Pd ratios, however, none of the compositions yield the observed high Re/Os ratios. Following this the initial impact melt (silicate melt and metal) would have lost almost half of its iron content and roughly 60% of the HSE. Hence, complementary to the fractionated late stage metallic liquids which remain in the impact melts, large amounts of segregated Fe-Ni metal would have been produced. Its unique HSE composition (high absolute concentrations and relative enrichment of refractory HSE) and redistribution by subsequent impacts would make it relatively unlikely to overlook such compositions. However, such fractionated solid metal has never been sampled on the lunar surface or in lunar meteorites. In contrast, sampled lunar impact melt rocks containing abundant metal spherules display the most fractionated HSE pattern (Fischer-Gödde and Becker, 2012; Liu et al., 2015; this study). Furthermore, the measured $^{187}Os/^{188}Os$ ratios are positively correlated with their Os concentration, which strongly precludes their interpretation as result of fractionation of Re from Os during large-scale igneous differentiation of impact melt pools (Fig. 7). Textural observations and the solid metal-liquid metal partitioning models of the HSE strongly suggest that Fe-Ni metal-schreibersite-troilite spherules in impact melt rocks are neither exotic grains segregated from upper portions of a cooling impact melt sheet nor solidified residual liquids after fractional crystallization of large amounts of solid metal. Instead they are generated by small-scale fractional crystallization of these phases from immiscible metallic liquid which after major silicate crystallization cooled below the eutectic temperature of the Fe(Ni)-P-S system. The HSE record preserved in the metal, phosphide and sulfide phases is therefore regarded as representative of the impact melt (i.e. impactor-target mixture) in which they crystallized. However, it is worth to note here that analyzes of single grains or *in situ* analyses will be strongly affected by the above discussed small-scale processes.

From the HSE record alone, it is not possible to exclude the idea of large-scale fractional crystallization of thick impact melt sheets, especially when only silicate phases are involved. However, in contrast to slowly-crystallized cumulate rocks, the majority of Apollo 16 impact melt rocks display fine-grained subophitic to intersertal textures, often referred to as basaltic (e.g. 62295), and thus separation and accumulation of solid metal likely was not efficient because of fast initial cooling rates. The only exception may be a recently documented coarse-grained (by lunar standards) cumulate rock formed by fractional crystallization in a lunar impact melt sheet (Norman et al., 2016). These authors argue that high abundances of siderophile element-rich metal makes early metal segregation unlikely

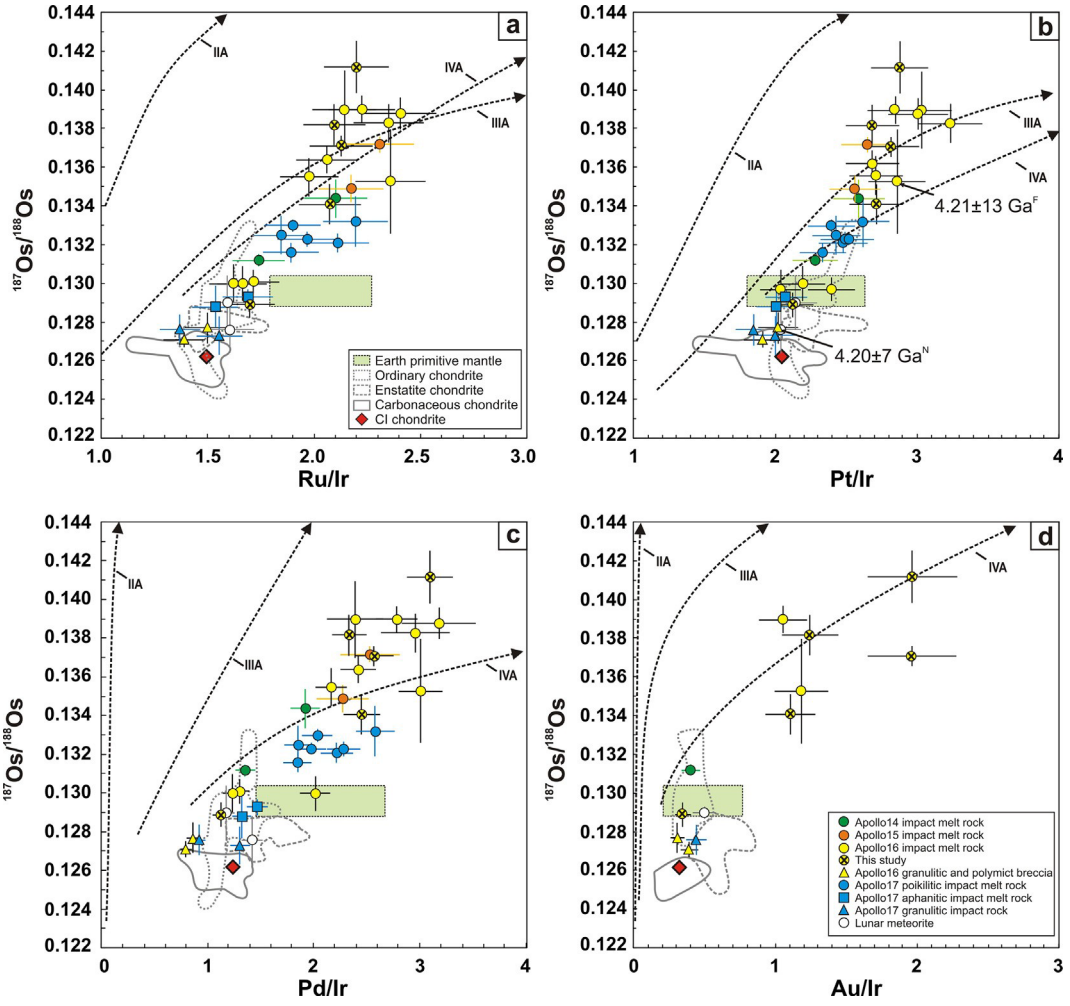

Fig. 5. Bulk HSE/Ir ratios vs. osmium isotopic ratios of lunar impact rocks. All HSE/Ir ratios are calculated from weighted average values and uncertainties reflect the overall precision of concentration determinations (7% for Ru, Pt and Pd and 16% for Au). $^{187}Os/^{188}Os$ ratios are weighted averages and uncertainties are $2\sigma_m$. Isotope dilution multiple aliquot HSE data taken from Puchtel et al. (2008), Fischer-Gödde and Becker (2012), Sharp et al. (2014), Liu et al. (2015) and this study. Age data are: ^{N}Sm-Nd isochron age of granulitic impactite 67955 (Norman et al., 2016) and ^{F}Re-Os isochron age of subophitic impact melt rock 67935 (Fischer-Gödde and Becker, 2012). The range of the terrestrial primitive mantle (Meisel et al., 2001; Becker et al., 2006; Fischer-Gödde et al., 2011), chondrite classes (Horan et al., 2003; Fischer-Gödde et al., 2010) and fractionation trends of magmatic iron meteorite groups (Pernicka and Wasson, 1987; Hoashi et al., 1993; Cook et al., 2004; Petaev and Jacobsen, 2004; McCoy et al., 2011) are given for comparison.

in this specific sample and that fractional crystallization of lunar melt sheets may be less effective than predicted by recent models (see discussion in Norman et al., 2016). This interpretation is consistent with our model of late crystallization of metal-schreibersite-troilite aggregates from interstitial liquid metal droplets.

5.1.5. Implications for the determination of element ratios from multiple aliquots of impact rock samples

The HSE/Ir ratios derived from the regression of multiple aliquots of sample 62295 are identical within uncertainty to results obtained recently by Liu et al. (2015) on a different split of the same sample. The coherence in HSE/Ir ratios as well as in osmium isotopic composition (see Section 4.1.) obtained from two different ~1 g sample splits apparently demonstrates, that the aliquot method yields representative results for such impact melt rocks. However, Liu et al. (2015) obtained nonzero intercept values for Pt and Pd, whereas zero intercepts were observed in our study (Table 2). As was discussed before, HSE partitioning between solid metal and liquid metal reveals small-scale fractionation processes upon cooling and solidification of the impact melt rocks. The observed range in HSE/Ir ratios in mineral separates and rock aliquots is fully explained by this process. Therefore, results of the regression calculations reflect the variability of concentration data and HSE ratios, both of which depend mainly on size and distribution of metal grains in the impact melt rock and compositional differences inherited from the small-scale processes that produced them. Furthermore, the weight and HSE concentration of aliquots and their mass balance remains disregarded. This effect is small in samples where

the HSE are relatively homogeneously distributed, but rather large (up to 30%) when large metal particles are present (usually the case in non-chondritic impact melt rocks at the Apollo 16 landing site). The latter make bulk HSE/Ir ratios obtained from regression of multiple aliquot data highly susceptible to errors due to changes in their slope. Non-zero intercepts of regression calculations and deviations from true linearity, as observed in several impact melt rock studies, are therefore interpreted as the graphical expression of local small-scale fractionation processes and aliquoting, but seem to be unrelated to target contributions or physical mixing of HSE carrier phases of different impactors as suggested by some previous studies (e.g. Liu et al., 2015).

In order to obtain reliable element ratios, we use weighted averages of concentration determinations that include mineral separates. This approach represents the full element budget of gram-size samples, similar to Norman et al. (2002) where different aliquots of a homogenized sample powder were averaged. However, the analysis of multiple rock aliquots makes differences in absolute and relative abundances of HSE detectable, although heterogeneities due to solid metal-liquid metal partitioning need to be integrated to obtain bulk sample HSE ratios. For uncertainty estimation of HSE/Ir ratios obtained from weighted averages of our study we used error propagated 2r uncertainties of the concentration determinations for each element and aliquot. Resulting uncertainties are usually in the same range like those obtained from the regression method or lower when larger scatter in Ir vs. HSE diagrams is observed (Table. 2; Fig. 4). In order to compare our data, we calculated HSE/Ir ratios from weighted averages of literature values and assigned uncertainties using a common method (Figs. 5 and 6). The relative uncertainty of an element ratio was calculated as the root of the sum of squares of the overall precision of concentration determinations as reported in the data source. This method slightly overestimates uncertainties of precise concentration determinations, but might underestimate the uncertainties of less precise analyses, for example when blank contributions are high.

Comparing the results obtained by both methods for all available multi-aliquot ID data indicates some significant differences between the methods (Fig. 2 of the Electronic Supplement). Using strictly element ratios obtained by the regression method, apparently requires at least 3–4 components to explain the overall compositional variation of ancient lunar impactites. These compositions include a chondritic and a differentiated iron meteorite-like component, but also a component which in contrast to its highly radiogenic osmium isotopic composition (i.e. high Re/Os ratio) displays only slightly suprachondritic HSE/Ir ratios. The latter composition would be difficult to explain since no planetary or solar nebular fractionation process is known to produce it. In contrast, using element ratios obtained from weighted averages of concentration determinations shifts some of the data towards higher HSE/Ir ratios. The resulting distribution of element ratios obtained from weighted averaging displays a broadly linear array in HSE/Ir vs. $^{187}Os/^{188}Os$ plots (Fig. 5). As indicated by the systematic differences in HSE ratios of bulk lunar impactites calculated by the different approaches and the causes of systematic errors (discussed above), we conclude that the regression approach applied to samples that display coarse metal grains and underwent small-scale fractionation yields ratios, which in contrast to their apparent precision, are less accurate than ratios obtained from weighted averages. For the purpose of impactor characterization and identification of mixing proportions between different compositions, we therefore use weighted average values only (Figs. 4–6). The combination of both, either the regression method when justified by good correlation or averages when the scattering of measured aliquot data is too large, is not recommended since this may introduce apparent compositional trends for bulk samples which are artifacts.

5.2. Lunar impact processes and composition of the late accreted material

Detailed investigation of lunar impact rocks from different landing sites, employing precise isotope dilution methods, indicated a broadly linear correlation between HSE/Ir and $^{187}Os/^{188}Os$ ratios (Puchtel et al., 2008; Fischer- Gödde and Becker, 2012; Sharp et al., 2014; Liu et al., 2015). However, no consensus was reached on the interpretation of these data. The main questions are whether the detected range in compositions reflects the signature of different dominant impactor compositions (Sharp et al., 2014; Liu et al., 2015) or the mixing of different ancient impactor components (Fischer-Gödde and Becker, 2012) or both. In addition, the relative abundances of HSE in most lunar impactites plot outside the range of known chondritic meteorites, which is discussed in terms of either signatures of bulk chemical compositions that have not been sampled by primitive meteorites or by incorporation of differentiated metal from one or several fractionated planetesimal cores (Fischer-Gödde and Becker, 2012; Liu et al., 2015). In the following, new evidence from the present study will be discussed to address these hypotheses.

5.2.1. Osmium isotope constraints on impact rock formation and bombardment history

The overall suprachondritic average $^{187}Os/^{188}Os$ ratios of many Apollo 16 impact melt rocks support their formation from impact melts that contained a differentiated metal component (i.e. high long term Re/Os). However, the internal Re-Os systematics of subsamples and mineral separates of our study are inconsistent with reported Ar-Ar and Pb-Pb ages ranging from 3.64 to 4.08 Ga. Instead the Re-Os data suggest variable disturbance and resetting of the Re-Os system (Fig. 1).

Sample 62295 displays strong evidence for element mobility and open system behavior. Although rust was not reported (Hunter and Taylor, 1981) differences between Re and Re^* reveal that some alteration process must have taken place which redistributed Re to variable amounts and led to a late-stage Re loss of approximately 6.5%. The possibility of an overestimation of Re abundances due to cosmic ray induced Re isotopic anomalies was evaluated in previous studies (Day et al., 2010; Fischer-Gödde

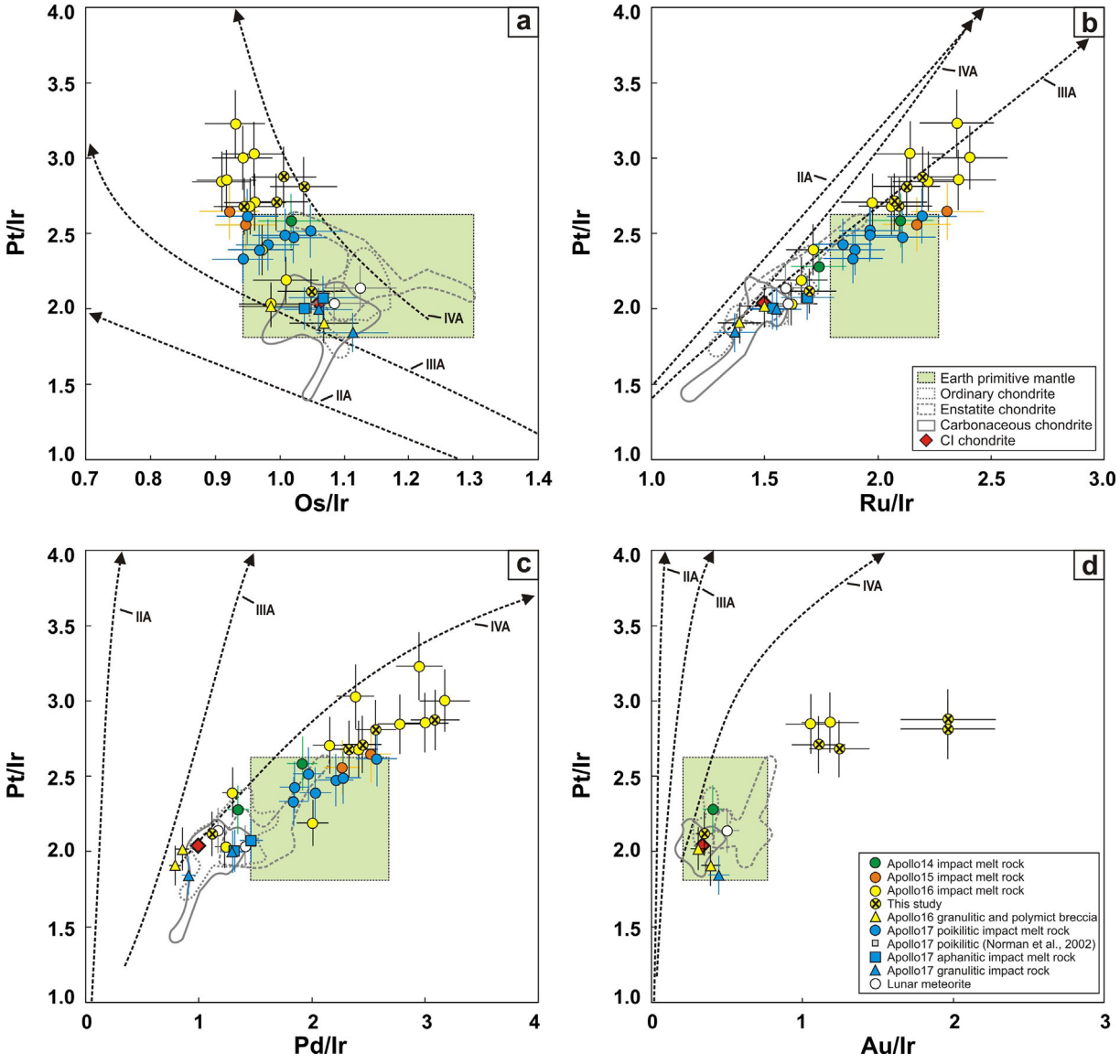

Fig. 6. Bulk HSE/Ir ratios of lunar impact rocks. Data source for lunar samples and the terrestrial primitive mantle as well as meteorite compositions as in Fig. 5.

and Becker, 2012; Liu et al., 2015). Although, the W/Re ratios of subsamples are not exactly known, the possible effects are likely smaller than the analytical uncertainty of the Re concentration determination (Fischer-Gödde and Becker, 2012).

The Re-Os systematics of sample 61016 reflects its complex history. The Os concentration of the impact melt portion is strongly diluted by anorthositic glass without any measurable effect on its isotopic composition (Fig. 1e). The isotopic record of two splits of a lithic clast can be attributed to mm-scale heterogeneities within the rock. Variable Re and Os partition coefficients between different minerals lead to variable time-integrated in-growth of ^{187}Os in separates. A similar Re-Os fractionation was observed for MGS norite sample 15455 (Day et al., 2010). Averaging our data obtained on both splits of the lithic clast yields 1.8 ng/g Ir, $^{187}Os/^{188}Os = 0.119 \pm 16$ and CI chondritic refractory HSE/Ir within uncertainties. The moderately volatile HSE and sulfur display a fractionated normalized pattern, with highest concentrations for sulfur. Earlier RNAA data showed that the light-colored anorthositic part of 61016 contains no meteoritic material, although it is described as strongly being enriched in some volatile elements, interpreted to reflect fumarolic enrichment after crystallization and brecciation (Ganapathy et al., 1973; Krähenbühl et al., 1973).

Internal isochron ages obtained from rock and mineral separate aliquots of 65055 and 60335 yield 2.45 ± 0.56 Ga and 3.09 ± 0.42 Ga, both significantly younger than the published Ar-Ar age of 3.82 ± 0.03 Ga (Haber et al., 2014) and the Pb-U-Th model age of 4.08 Ga (Barnes et al., 1973). The uncertainties of the age data are large

because of limited spread in Re/Os ratios and scatter beyond analytical uncertainties. Hunter and Taylor (1981) reported traces of rust in 60335 which is possibly the reason for scatter and deviation of two data points from the isochron. However, differences between the average values of measured Re and calculated Re^* are below (65055) or only slightly exceed (60335) uncertainties of concentration determinations (Table 1), indicating that both samples remained almost entirely closed systems and that the age data are reliable. Based on the modeling of HSE partitioning the possibility of mixing and incomplete equilibration of metal of different provenance during formation of 60335 can be excluded (see Section 5.1.4.). Initial $^{187}Os/^{188}Os$ ratios are consistent with the overall HSE characteristics of the samples (chondritic in 65055 and suprachondritic in 60335) indicating the early formation of these patterns.

Full or partial resetting of the Re-Os system in Apollo 16 impactites was most likely achieved by thermal events like late impacts. Shuster et al. (2010) inferred thermal disturbance of Apollo 16 regolith samples at ~3.3 Ga. The latter authors argue that the Ar diffusion kinetics of different lithologies is consistent with a short-duration heating event (300–600 °C) at that time. Liu et al. (2015) reported a Re-Os isochron age of 2.97 ± 0.40 Ga for a basaltic impact melt breccia whose formation was dated at ~3.9 Ga using the Ar-Ar technique. Although sampled at different stations, the latter age is identical with the re-equilibration date of sample 60335. The younger apparent age of 65055 may be consistent with the timing of local impacts near the Apollo 16 landing site (Joy et al., 2011). The large uncertainties of the obtained Re-Os ages hamper further stratigraphic interpretation, but their Re-Os systematics is consistent with impact induced heating due to a close-by impact or burial by hot impact ejecta long after the basin forming period.

5.2.2. Origin of bulk HSE compositions of Apollo 16 impactites

Phase relations and HSE partitioning modeling discussed in previous sections strongly suggest that upon solidification metal-schreibersite-troilite aggregates in the impact melt remained closed systems on the sub-cm-scale. Hence, the observed relative HSE composition preserved in a specific impact melt rock should directly reflect the composition of the impactor-target mixture without modifications by large-scale fractionation processes. One of the main questions in studies of lunar impactites is whether the impacting material was of primitive or differentiated composition and whether or not compositions are similar to those in meteorite collections. These questions arise because material accreted during the early history of the terrestrial planets may have had a different composition compared to recent meteorite falls and finds derived from the main asteroid belt (e.g. Wetherill, 1985), which may not sample the full spectrum of inner solar system materials.

Recent studies of components in highly unequilibrated ordinary and enstatite chondrites reveal that some metal fractions may be up to 30% more fractionated in HSE ratios when compared to their respective bulk compositions (e.g., Horan et al., 2009; Kadlag and Becker, 2015). Their osmium isotopic compositions demonstrate that this fractionation took place very early in the solar system history and hence, differences between chondrite groups may reflect the presence of variable proportions of components that formed in different environments of the solar nebula (Horan et al., 2009; Kadlag and Becker, 2015). Following this idea, primitive impactor compositions 10–30% more fractionated in refractory elements than bulk rocks of known chondrite groups may have existed. HSE patterns observed in Apollo 14 and 17 impact melt rocks may be explained by such hypothetical primitive impactor composition, but likely not the more strongly fractionated Apollo 15 and 16 samples (Fig. 6). In addition, none of the known chondrite components display $^{187}Os/^{188}Os$ ratios (i.e. long term Re/Os ratios) as high as most of the Apollo 16 impact melt rocks (Fig. 5) and therefore a fractionation mechanism different from chondrite component formation processes may be required.

As suggested before, the HSE record of non-chondritic impact melt rocks may represent fractionation processes involving metal–silicate differentiation and solid metal-liquid metal fractionation during core formation and core solidification on the parent bodies of impactors (Fischer- Gödde and Becker, 2012). Four of the studied impact melt rocks together with samples analyzed by Fischer-Gödde and Becker (2012) and Liu et al. (2015) display suprachondritic $^{187}Os/^{188}Os$ ratios, increasingly suprachondritic HSE/Ir ratios from refractory to moderately volatile HSE, enrichment of normalized Ru over Pt and depletions in sulfur (Figs. 4a and 5). This group of non-chondritic impact melt rocks displays also a higher KREEP component and is clearly distinct from KREEP-poor impactites and samples from other landing sites (Fig. 4b). The non-chondritic Apollo 16 impactites themselves display considerable variations in HSE/Ir, S/Ir and $^{187}Os/^{188}Os$ ratios. These variations increase from refractory (~20%) to moderately volatile HSE (>40%) and preclude their designation as signature of a single dominant iron meteorite impactor composition into HSE-poor target material (Figs. 5–7).

In contrast to the non-chondritic impact melt rocks, sample 65055 and three samples analyzed by Liu et al. (2015) differ only slightly from chondritic ratios (Fig. 4a) and display chondritic $^{187}Os/^{188}Os$ ratios in the narrow range from 0.129 to 0.130 (Fig. 5). All members of this group are clast-free coherent, subophitic-intersertal impact melt rocks, classified as feldspatic group 3 (Korotev, 1994) and bear only a minor KREEP component (Vaniman and Papike, 1980; McKinley et al., 1984). Available Rb-Sr and Ar-Ar data for these samples indicate a relative young formation age at ~3.82 ± 0.02 Ga (Papanastassiou and Wasserburg, 1972; Deutsch and Stöffler, 1987; Norman et al., 2006; Haber et al., 2014). Assuming a common impact origin, the HSE record of these samples may represent the signature of an approximately chondritic impactor, similar to ordinary or enstatite chondrites (Liu et al., 2015). However, apart from their relatively unfractionated HSE pattern, the samples display two complementary compositional features which argue against this interpretation. All samples are slightly enriched in normalized Ru over Pt which is a characteristic feature of the non-chondritic

KREEP-rich Apollo 16 impact melt rocks, whereas 65055 displays a depletion in Pd, similar to granulitic and polymict impact breccias (Fischer-Gödde and Becker, 2012). Based on these observations and their intermediate lithophile trace element content, the composition of these samples can be fully explained by mixing of large amounts of KREEP-poor feldspatic impactites with chondritic HSE ratios and minor KREEP-rich non-chondritic impactites. A similar assimilation process was recently documented in Apollo 17 aphanitic melt breccias which display a mixed HSE budget due to granulitic clasts with chondritic HSE ratios that were incorporated into non-chondritic impact melt, but not entirely molten at the time of impact melt crystallization (Sharp et al., 2014).

The distinct HSE and osmium isotopic compositions of Apollo 17 poikilitic melt rocks and available data for two Apollo 15 impact melt rocks were interpreted as signatures of two dominant impactors which formed the Serenitatis (Puchtel et al., 2008; Sharp et al., 2014) and the Imbrium basin (Liu et al., 2015). Based on similarities of HSE pattern to non-chondritic Apollo 16 samples (Fig. 4b) and the broadly linear correlation of HSE/Ir and $^{187}Os/^{188}Os$ ratios from all landing sites (Figs. 5 and 6) the alternative interpretation of variable mixing of a slightly volatile element depleted carbonaceous chondrite-like compositions, as reflected by the granulite suite, with suprachondritic iron meteorite-like compositions reflected by the non-chondritic Apollo 16 impact melt rocks, as suggested by Fischer- Gödde and Becker (2012), appears possible. If the latter model is correct, similar meteoritic components were mixed in somewhat different ratios in impact rocks from all Apollo mission landing sites. However, this interpretation requires a process which transported and mixed impactor material at least on the scale of the lunar near-side where the samples were collected. Formation ages of 4.21 ± 0.13 Ga and 4.20 ± 0.07 Ga (Fischer-Gödde and Becker, 2012; Norman et al., 2016) determined for two impact melt rocks of contrasting HSE composition (Fig. 5b) support their formation in different basin-scale impact events. Most other impact rocks, regardless of the sampling location plot in between these ancient compositions (Fig. 5), whereas their Ar-Ar ages are mostly younger due to isotopic resetting (Norman et al., 2006; Shuster et al., 2010; Fernandes et al., 2013). Thus, at least two early basin forming events are recorded by their different HSE signature in Apollo 16 impactites. Mixing, remelting and homogenization may have been aided by younger impact events and the redistribution of older ejecta (e.g. Norman et al., 2010; Fernandes et al., 2013).

Virtually all of the non-chondritic impactites bear significant amounts of KREEP component (Fig. 4b), indicating assimilation of the latter during one or several early impacts of differentiated impactor material. The apparent correlation of HSE fractionation with lithophile trace elements like U or Rb, as an indicator of the KREEP component (e.g. Hertogen et al., 1977), seems to reflect a later dilution process with KREEP-poor crust and chondritic impactor material (see discussion above). The origin of the KREEP component and the place and formation process of non-chondritic impactites is beyond the scope of this contribution. However, quantitative assessment of ancient meteoritic components and their mixture on the lunar surface require more precise knowledge about the nature of the non-chondritic impactor composition which seems to be

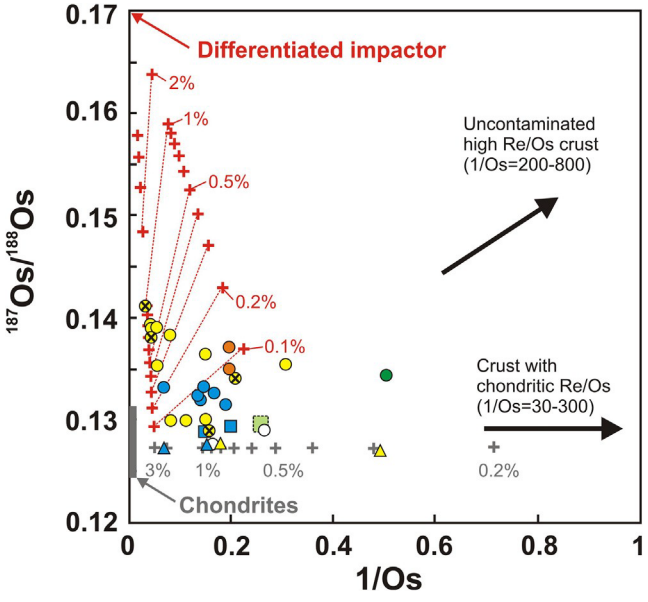

Fig. 7. $^{187}Os/^{188}Os$ ratios plotted against 1/Os for ancient lunar impact rocks from Apollo 14, 15, 16 and 17 landings site and lunar meteorites. Uncertainties were omitted for the sake of clarity of the figure. Data source and symbols as in Fig. 5. Mixing calculations are displayed for increments of 0.1 from 0.2 to 1 wt.% and 1 from 1 to 3 wt.% of an average-chondrite impactor composition (0.7 μg/g Os; $^{187}Os/^{188}Os$ = 0.1275; gray symbols) with average high Re/Os lunar crust (3 ng/g Os; $^{187}Os/^{188}Os$ = 0.174). Further mixing with an assumed differentiated impactor composition (1 μg/g Os; $^{187}Os/^{188}Os$ = 0.17; red symbols) starts from 0.5 wt.% and 3 wt.% of the crust-chondrite mixture.

diluted by chondritic material in almost all lunar impactites.

Many lunar impact melt rocks display characteristic fractionated HSE signatures which broadly compare to iron meteorites like fractionated members of the IVA or IIIA group (Morgan et al., 1972; Fischer-Gödde and Becker, 2012; Liu et al., 2015). However, none of these meteorite compositions provide a full match to all HSE/Ir ratios (Fig. 6). Just as in small-scale processes during impact melt solidification (see discussion in Section 5.1.4.), large-scale fractionations in HSE compositions of magmatic iron meteorites are a function of light element abundances of the metallic liquid (e.g. Wasson, 1999; Chabot and Drake, 2000; Wasson et al., 2007; McCoy et al., 2011). Therefore, specific HSE compositions observed in impactites can be diagnostic of the conditions of core crystallization on the differentiated parent body of the impactor.

As shown before, non-chondritic Apollo 16 impact melt rocks display HSE fractionations typical for residual metallic liquids after fractional crystallization of solid metal. These features are moderately suprachondritic Re/Os ratios, increasingly suprachondritic HSE/Ir from refractory to moderately volatile HSE and a characteristic enrichment of normalized Ru/Ir over Pt/Ir (i.e., suprachondritic Ru/Pt, Fig. 4a). The latter feature seems to evolve only if the light element content and P/S ratio of the initial melt are high enough (see discussion in Section 5.1.3.). For the most common magmatic iron meteorites groups, initial sulfur contents of 2–7.5 wt.% and a narrow range of P/S ratios from 0.20 to 0.24 were estimated (Wasson, 1999; Wasson et al., 2007; McCoy et al., 2011). Following this, the characteristic HSE fractionations preserved in non-chondritic Apollo 16 impact melt rocks reflect that of residual metallic liquid after significant solid core formation from metal melt initially rich in light elements and a P/S ratio higher than 0.24.

Fe-Ni metal of main group pallasites formed by fractional crystallization of solid metal, like magmatic iron meteorites, albeit of higher initial P content and P/S ratio in the metal melt (Boesenberg et al., 2012 and references therein). Evolved metal compositions found in some pallasites display fractionated HSE patterns which are representative of fractionation processes during core solidification of such parent bodies (Lee et al., 2006; Danielson et al., 2009). In a simple mixing model, the bulk metal HSE composition of main group pallasite Cumulus Ridge (Danielson et al., 2009) would produce most of the compositions observed in non-chondritic Apollo 16 impact melt rocks (Fig. 4c; details of end-member compositions in these and the following models are given in Table 3 of the Electronic Supplement). However, we like to emphasize here that we do not propose the latter meteorite composition or pallasites in general as dominant differentiated impactor composition on the Moon. Instead, the latter model demonstrates that large-scale fractionation processes during solid metal crystallization from metal melt high in phosphorous can produce the inferred impactor composition.

P/S ratios of primitive meteorites are restricted to relatively low values (0.017–0.052), however, the terrestrial planets may have higher P/S because of the possibility of a stronger depletion of the more volatile elements such as S (e.g. Palme and O'Neill, 2003). The physical conditions of metal–silicate segregation and resulting differences in metal–silicate partitioning behavior between both elements are also an important control on initial P/S ratios of the metal melt. During asteroidal core formation metal–silicate equilibrium is mainly controlled by pressure and oxygen fugacity conditions where P and S follow opposite trends for both parameters (Schmitt et al., 1989; Rose-Weston et al., 2009; Boujibar et al., 2014). Experimental data suggest that higher P/S ratios in metal melt can reflect a more volatile depleted parent body composition or lower oxygen fugacity and/or lower equilibration depth during core formation, or a combination thereof.

In order to explain the origin of the observed HSE compositions in lunar impactites in general, a three component mixing model was applied. We used the concentration of Os as measure for the overall contribution from meteoritic material to the pristine lunar crust and its isotopic composition as a proxy for the amount of differentiated impactor component (Fig. 7). For the sake of clarity of the model, we calculated average chondritic meteorite addition first (0.7 μg/g Os; $^{187}Os/^{188}Os = 0.1275$), although the real impact history may have been more complex. In contrast to chondrites, which display a narrow range in Os concentrations and isotopic compositions (Horan et al., 2003; Fischer-Gödde et al., 2010), the choice of the differentiated impactor component has a stronger influence on the outcome of compositional mixtures. In order to fulfill the constraints from liquid metal-solid metal partitioning of a light element rich core composition with high P/S ratio (see discussion above) we assumed a metal composition which is moderately high in HSE, but fractionated in relative abundances (1 μg/g Os; $^{187}Os/^{188}Os = 0.17$). When compared to magmatic iron meteorite data such composition is similar to IIA Filomena, but a higher P/S ratio of the metal melt would fractionate the HSE, similar to what is observed in main group pallasites like Cumulus Ridge (Fig. 4c). The assumed radiogenic $^{187}Os/^{188}Os$ ratio is consistent with high long term $^{187}Re/^{188}Os$ ratios as reported by Lee et al. (2006).

Adding very small amounts of chondritic impactor material to low HSE lunar crust drastically lowers its $^{187}Os/^{188}Os$ ratio and minor chondritic contamination of ancient lunar crustal rocks seems prevalent (Day et al., 2010). In our model, the composition of granulitic impactites and polymict breccias is explained by the addition of 0.3 to 3 wt.% of average chondritic material (Fig. 7). All other samples, mainly impact melt rocks from different landing sites, display more radiogenic Os isotopic compositions and require an addition of a non-chondritic impactor component. In order to account for net-contents of chondritic impactor material we calculated two mixing lines starting from 0.5 and 3 wt.%. We realize the limitations of this approach; however, the majority of the impactites are explained by less than 1.5 wt.% addition of the assumed differentiated impactor component. These estimates are in broad agreement with observed contents of Fe-Ni metal in impact melt rocks (e.g. Misra and Taylor, 1975;

Hunter and Taylor, 1981). From these calculations, it becomes clear that none of the impactites (not even the most fractionated ones) are free of chondritic impactor component. Samples that fall outside the field of calculated mixing relations (i.e. lower Os concentrations) reflect lower absolute meteoritic contributions, but are roughly similar ratios between chondritic and differentiated component. Following the above model, consideration of a chondritic and a differentiated impactor component fully explains the correlation of HSE ratios and $^{187}Os/^{188}Os$ ratios which are observed in lunar impactites from Apollo 14, 15, 16 and 17 landing site (Figs. 5 and 6).

5.2.3. Constraints on the composition of material accreted late to the Moon and Earth

The observed range in HSE and $^{187}Os/^{188}Os$ ratios of lunar impactites (Puchtel et al., 2008; Fischer-Gödde and Becker, 2012; Sharp et al., 2014; Liu et al., 2015) reflect the accretion of chondritic and non-chondritic impactor material onto the lunar crust. The non-chondritic component may contribute up to ~30 wt.% of the HSE budget of the most fractionated impactites (i.e. Apollo 16 impact melt rocks). The apparent predominance of a single non-chondritic component (or the virtual absence of other differentiated impactor compositions) and its prevalence in KREEP-rich rocks (e.g. Hertogen et al., 1977) remains enigmatic. A possible explanation might be, that accretion of chondritic material was interrupted by a single basin sized impact of non-chondritic material into KREEP-rich crust of the lunar nearside (indicated by tie-lines in Fig. 7). The alternative interpretation of accretion of various smaller impactors of very similar fractionated composition seems less likely, especially in the light of the specific constraints on their formation discussed in the previous section.

Meteoritic contamination is prominent among lunar impactites (0.5–30 ng/g Ir and Au/Ir = 0.3–2), lunar meteorites (1–20 ng/g Ir and Au/Ir = 0.3–2; Korotev, 2003) and in regolith and soil samples (2–20 ng/g Ir and Au/Ir = 0.3–1; Haskin and Warren, 1991), and the non-chondritic component seems to occur widespread. However, the absolute mass of accreted material in lunar ejecta deposit, regolith and the deep crust is uncertain. In order to estimate the late accreted mass in the crust, we assume that either 10% (the uppermost ~5 km) or more conservative 2% (the uppermost 1 km) of lunar crust was affected by late accretion after the formation of a thick lunar crust. Since the global distribution of the non-chondritic component and its relative amount is not well known we only consider chondrite-like impactor addition here. From the data available (see above) we assume 10 ng/g Ir in the impact contaminated crustal sections, which equals to ~2 wt.% of on average chondrite-like contaminants. Following these assumptions, we calculated late accretion to the lunar crust of $2 * 10^{18}$ and $1 * 10^{19}$ kg, respectively. Based on late accretion estimates of $1.5 * 10^{19}$ kg to the source of lunar mare basalts (Day and Walker, 2015) this could correspond to 10 wt.% or 40 wt.% of the bulk late accretion to the Moon (i.e. late accretion to lunar mantle and crust). However, the results of the latter model are strongly dependent on assumptions on the average thickness of affected crustal sections and mantle chemistry. Following the results of our model and the relatively shorter time interval of late accretion to the lunar mantle (see discussion in Day and Walker, 2015) the average accretion rate declines by one order of magnitude after formation of a thick lunar crust. This is consistent with recent estimations on the timeline of lunar basin formation (Morbidelli et al., 2012).

A considerable larger mass fraction of ~0.5 wt.% of its present mass was accreted to Earth (Becker et al., 2006; Walker et al., 2015). In order to account for the difference of late accreted mass, disproportional late accretion to Earth and Moon was proposed to have been caused by stochastic accretion of large bodies to the Earth (Bottke et al., 2010). This model is consistent with the recently discovered excess of 20–27 ppm inferred for lunar ^{182}W compared to the BSE (Kruijer et al., 2015; Touboul et al., 2015). Based on the relative abundances of siderophile and chalcophile elements of the BSE, the overall composition of the late accreted material was estimated as chemically similar to carbonaceous-chondrite with a minor proportion of non-chondritic siderophile element-rich material (Becker et al., 2006; Walker et al., 2015; Fischer-Gödde and Becker, 2012; Wang and Becker, 2013). The HSE composition of the BSE displays similar- ities to characteristic element ratios which were observed in non-chondritic lunar impact melt rocks, particularly high Ru/Pt and Pd/Pt ratios. Following this and the results of the present study, the Earth may have received a minor fraction of material of similar origin as in the Apollo 16 impactites during late accretion. However, alter- native explanations like a residual signature of sulfide- silicate partition (Laurenz et al., 2016) or contamination of the mantle with outer core material (Rose-Weston et al., 2009) may also provide explanations and need to be explored further.

6. SUMMARY

Fe-Ni metal-schreibersite-troilite intergrowths which were observed in Apollo 16 impact melt rocks crystallized from immiscible liquid metal droplets in silicate impact melts. These intergrowths underwent fractional crystallization at the sub-centimeter-scale which resulted in compositional variations and strong differences in absolute and relative HSE abundances of the different phases. This process is the main reason for variations in HSE/Ir ratios observed in 1–100 mg-aliquots of gram-size fragments of lunar impact melt rocks. Bulk HSE/Ir ratios derived from regression of multiple aliquot data are therefore prone to larger errors and might lead to inaccurate results. Weighted averages of concentration data of aliquots account for the full element budget of all analyzed aliquots and yield more accurate HSE/Ir ratios of the bulk sample.

Modeling of solid metal-liquid metal partitioning in the Fe-Ni-S-P system reveals that fractionated HSE compositions as observed in the samples studied, are representative of liquid metal compositions in the impact melts and that fractional crystallization on the scale of large impact melt pools most likely did not occur. The HSE compositions

are therefore in principle useful for impactor discrimination and study of impact and mixing processes.

The compositional record of Apollo 16 impactites show a mixture of chondritic and a non-chondritic impactor signature, represented by granulitic impactites and KREEP-rich impact melt rocks with strongly fractionated HSE. This observation and the broadly linear correlation between ^{187}Os/^{188}Os ratios and HSE/Ir ratios in impactites from all Apollo landing sites, supports the interpretation of variable mixing of chondrite-like impactor material with suprachondritic iron meteorite-like impactor material, and subsequent homogenization by younger impacts, as proposed by Fischer-Gödde and Becker (2012). Our data together with recent findings by Fischer-Gödde and Becker (2012) and Liu et al. (2015) show that disturbance and sometimes complete internal resetting of the Re-Os system in gram-size samples is relatively easily achieved by later impact and heating events, whereas the Ar-Ar system is less affected and might still display older ages.

Non-chondritic Apollo 16 impact melt rocks display characteristic features like high Re/Os (and corresponding moderately suprachondritic ^{187}Os/^{188}Os ratios), increasingly suprachondritic HSE/Ir ratios from refractory to moderately volatile and suprachondritic Ru/Pt. These characteristics are interpreted to reflect large-scale fractional crystallization of solid metal from metal melt during core solidification in the parent body of one or several putative impactors. The observed HSE fractionation and the characteristic enrichment of Ru over Pt when normalized to CI chondrite values strongly indicates a light element-rich metal melt with a P/S ratio higher than in most iron meteorite parent bodies. Although, such compositions were only sampled in some main group pallasites, the occurrence of a similar Ru (and Pd) anomaly in the BSE (Becker et al., 2006) suggests that the material accreted late to Earth possibly contained a considerable fraction of material of similar origin.

ACKNOWLEDGEMENTS

The authors wish to thank CAPTEM and the Lunar Sample Curator for sample allocation, F. Mangels for performing some of the chemical separations in the laboratory. Thoughtful reviews by Mario Fischer-Gödde and an anonymous reviewer, as well as editorial handling by Richard Walker are gratefully acknowledged. This work was funded by the Deutsche Forschungsgemeinschaft (BE1820/11-1, SFB-TRR 170, subproject B1-1). This is TRR 170 Publication No. 2.

APPENDIX A. SUPPLEMENTARY DATA

Supplementary data associated with this article can be found, in the online version, at http://dx.doi.org/10.1016/j.gca.2016.12.017.

REFERENCES

Barnes I. L., Garner E. L., Gramlich J. W., Machlan L. A., Moody J. R., Moore L. J., Murphy T. J. and Shields W. R. (1973) Isotopic abundance ratios and concentrations of selected elements in some Apollo 15 and Apollo 16 samples. *Proc. Lunar Sci. Conf.* 4, 1197–1207.

Becker H., Horan M. F., Walker R. J., Gao S., Lorand P. and Rudnick R. L. (2006) Highly siderophile element composition of the Earth's primitive upper mantle: Constraints from new data on peridotite massifs and xenoliths. *Geochim. Cosmochim. Acta* 70, 4528–4550.

Birck L., Roy-Barman M. and Capmas F. (1997) Re–Os isotopic measurements at the femtomole level in natural samples. *Geostand. Newslett.* 21, 19–28.

Boesenberg J. S., Delaney J. S. and Hewins R. H. (2012) A petrological and chemical reexamination of main group pallasite formation. *Geochim. Cosmochim. Acta* 89, 134–158.

Bottke W. F., Levison H. F., Nesvorný D. and Dones L. (2007) Can planetesimals left over from terrestrial planet formation produce the lunar Late Heavy Bombardment? *Icarus* 190, 203–223.

Bottke W. F., Walker R. J., Day J. M. D., Nesvorný D. and Elkins-Tanton L. (2010) Stochastic late accretion to Earth, the Moon, and Mars. *Science* 330, 1527–1530.

Boujibar A., Andrault D., Bouhifd M. A., Bolfan-Casanova N., Devidal J.-L. and Trcera N. (2014) Metal-silicate partitioning of sulphur, new experimental and thermodynamic constraints on planetary accretion. *Earth Planet. Sci. Lett.* 391, 42–54.

Chabot N. L. and Drake M. J. (2000) Crystallization of magmatic iron meteorites: The effects of phosphorus and liquid immiscibility. *Meteorit. Planet. Sci.* 35, 807–816.

Chabot N. L., Wollack E. A., McDonough W. F. and Ash R. (2014) The effect of light elements in metallic liquids on partitioning behavior. Lunar Planet. Sci. 45th. Lunar Planet. Inst., Houston. #1165(abstr.).

Chabot N. L., Saslow S. A., McDonough W. F. and Jones J. H. (2009) An investigation of the behavior of Cu and Cr during iron meteorite crystallization. *Meteorit. Planet. Sci.* 44, 505–519.

Cook D. L., Walker R. J., Horan M. F., Wasson J. T. and Morgan J. W. (2004) Pt–Re–Os systematics of group IIAB and IIIAB iron meteorites. *Geochim. Cosmochim. Acta* 68, 1413–1431.

Corrigan C. M., Chabot N. L., McCoy T. J., McDonough W. F., Watson H. C., Saslow S. A. and Ash R. (2009) The iron-nickel-phosphorous system: effects on the distribution of trace elements during the evolution of iron meteorites. *Geochim. Cosmochim. Acta* 73, 2674–2691.

Danielson L. R., Righter K. and Humayun M. (2009) Trace element chemistry of Cumulus Ridge 04,071 pallasite with implications for main group pallasites. *Meteorit. Planet. Sci.* 44, 1019–1032.

Day J. M. D. and Walker R. J. (2015) Highly siderophile element depletion in the Moon. *Earth Planet. Sci. Lett.* 423, 114–124.

Day J. M. D., Walker R. J., James O. B. and Puchtel I. S. (2010) Osmium isotope and highly siderophile element systematics of the lunar crust. *Earth Planet. Sci. Lett.* 289, 595–605.

Deutsch A. and Stöffler D. (1987) Rb-Sr-analyses of Apollo 16 melt rocks and a new age estimate for the Imbrium basin: Lunar basin chronology and the early heavy bombardment of the Moon. *Geochim. Cosmochim. Acta* 51, 1951–1964.

Dreibus G., Palme H., Spettel B., Zipfel J. and Wä nke H. (1995) Sulfur and selenium in chondritic meteorites. *Meteoritics* 30, 439–445.

Ebihara M., Wolf R., Warren P. H. and Anders E. (1992) Trace elements in 59 mostly highland Moon rocks. *Proc. Lunar Planet. Sci. Conf.* 22, 417–426.

Fernandes V. A., Fritz J., Weiss B. P., Garrick-Bethell I. and Shuster D. L. (2013) The bombardment history of the Moon as recorded by ^{40}Ar-^{39}Ar chronology. *Meteorit. Planet. Sci.* 48, 1–29.

Fischer-Gödde M. and Becker H. (2012) Osmium isotope and highly siderophile element constraints on ages and nature of meteoritic components in ancient lunar impact rocks. *Geochim. Cosmochim. Acta* 77, 135–156.

Fischer-Gödde M., Becker H. and Wombacher F. (2010) Rhodium, gold and other highly siderophile element abundances in chondritic meteorites. *Geochim. Cosmochim. Acta* 74, 356–379.

Fischer-Gödde M., Becker H. and Wombacher F. (2011) Rhodium, gold and other highly siderophile elements in orogenic peridotites and peridotite xenoliths. *Chem. Geol.* 280, 365–383.

Ganapathy R., Morgan J. W., Krähenbühl U. and Anders E. (1973) Ancient meteoritic components in lunar highland rocks: Clues from trace elements in Apollo 15 and 16 samples. *Proc. Lunar Sci. Conf.* 4, 1239–1261.

Gooley R. C., Brett R. and Warner J. L. (1973) Crystallization history of metal particles in Apollo 16 rake samples. *Proc. Lunar Sci. Conf.* 4, 799–810.

Haber T., Norman M. D., Bennet V. C. and Jourdan, F. (2014) Formation ages, cogenetic relations and formation processes of a set of Apollo 16 impact melt rocks. Lunar Planet. Sci. 45th. Lunar Planet. Inst., Houston. #1693(abstr.).

Haskin L. and Warren P. (1991) Lunar chemistry. In *Lunar sourcebook: A user's guide to the Moon* (eds. G. H. Heitken, D. T. Vaniman and B. M. French). Cambridge Univ. Press, Cambridge, pp. 357–448.

Hertogen J., Janssens M. J., Takahashi H., Palme H. and Anders E. (1977) Lunar basins and craters: evidence for systematic compositional changes of bombarding population. *Proc. Lunar Sci. Conf.* 8, 17–45.

Horan M. F., Walker R. J., Morgan J. W., Grossman J. N. and Rubin A. E. (2003) Highly siderophile elements in chondrites. *Chem. Geol.* 196, 5–20.

Hoashi M., Brooks R. R. and Reeves R. D. (1993) Palladium, platinum and ruthenium in iron meteorites and their taxonomic significance. *Chem. Geol.* 106, 207–218.

Hunter R. H. and Taylor L. A. (1981) Rust and schreibersite in Apollo 16 highland rocks: Manifestations of volatile-element mobility. *Proc. Lunar Sci. Conf.* 12, 253–259.

James O. B., Ash R. D., McDonough W. F., Puchtel I. S. and Walker R. J. (2007) Fractionation and volatile redistribution of siderophile elements in metal grains from lunar impact-melt breccia 76215. Lunar Planet. Sci. 38th. Lunar Planet. Inst., Houston. #1094(abstr.).

Joy K. H., Kring D. A., Bogard D. D., McKay D. S. and Zolensky M. E. (2011) Re-examination of the formation ages of the Apollo 16 regolith breccias. *Geochim. Cosmochim. Acta* 75, 7208–7225.

Kadlag Y. and Becker H. (2015) Fractionation of highly siderophile and chalcogen elements in components of EH3 chondrites. *Geochim. Cosmochim. Acta* 161, 166–187.

Korotev R. L. (1994) Compositional variation in Apollo 16 impact-melt breccias and inferences for the geology and bombardment history of the Central Highlands of the Moon. *Geochim. Cosmochim. Acta* 58, 3931–3969.

Korotev R. L. (2003) Feldspathic lunar meteorites and their implications for compositional remote sensing of the lunar surface and the composition of the lunar crust. *Geochim. Cosmochim. Acta* 67, 4895–4923.

Krähenbühl U., Ganapathy R., Morgan J. W. and Anders E. (1973) Volatile elements in Apollo 16 samples: Implications for highland volcanism and accretion history of the moon. *Proc. Lunar Sci. Conf.* 4, 1325–1348.

Kruijer T. S., Kleine T., Fischer-Gödde M. and Sprung P. (2015) Lunar tungsten isotopic evidence for the late veneer. *Nature* 520, 534–537.

Laurenz V., Rubie D. C., Frost D. J. and Vogel A. K. (2016) The importance of sulfur for the behavior of highly-siderophile elements during Earth's differentiation. *Geochim. Cosmochim. Acta* 194, 123–138.

Lee S. R., Walker R. J., McCoy T. J. and McDonough W. F. (2006) 187Re-187Os isotopic and highly siderophile element systematics of pallasites. Lunar Planet. Sci. 37th. Lunar Planet. Inst., Houston. #1167(abstr.).

Liu J., Sharp M., Ash R. D., Kring D. A. and Walker R. J. (2015) Diverse impactors in Apollo 15 and 16 impact rocks: evidence from osmium isotopes and highly siderophile elements. *Geochim. Cosmochim. Acta* 155, 122–153.

Luck J. M. and Allègre C. J. (1983) ^{187}Re-^{187}Os systematics in meteorites and cosmochemical consequences. *Nature* 302, 130–132.

Ludwig K. R. (2012) Isoplot 3.75 A Geochronological toolkit for Microsoft Excel. Berkeley Geochronology Center, Special Publication No. 5.

Mann U., Frost D. J., Rubie D. C., Becker H. and Audétat A. (2012) Partitioning of Ru, Rh, Pd, Re, Ir and Pt between liquid metal and silicate at high pressures and high temperatures - Implications for the origin of highly siderophile element concentrations in the Earth's mantle. *Geochim. Cosmochim. Acta* 84, 593–613.

McCoy T. J., Walker R. J., Goldstein J. I., Yang J., McDonough W. F., Rumble D., Chabot N. L., Ash R. D., Corrigan C. M., Michael J. R. and Kotula P. G. (2011) Group IVA irons: new constraints on the crystallization and cooling history of an asteroidal core with a complex history. *Geochim. Cosmochim. Acta* 75, 6821–6843.

McKay G. A., Kridelbaugh S. J. and Weill D. F. (1973) The occurence and origin of schreibersite-kamacite intergrowths in microbreccia 66055. *Proc. Lunar Planet. Sci. Conf.* 4, 811–818.

McKinley J. P., Taylor G. J. and Keil K. (1984) Apollo 16: Impact melt sheets, contrasting nature of Cayley Plains and Descates Mountains, and geologic history. *Proc. Lunar Planet. Sci. Conf.* 14, 513–524.

Misra K. C. and Taylor L. A. (1975) Characteristics of metal particles in Apollo 16 rocks. *Proc. Lunar Sci. Conf.* 6, 615–639.

Meisel T., Walker R. J., Irving A. J. and Lorand J. P. (2001) Osmium isotopic compositions of mantle xenoliths: A global perspective. *Geochim. Cosmochim. Acta* 65, 1311–1323.

Morbidelli A., March S., Bottke W. F. and Kring D. A. (2012) A sawtooth-like timeline for the first billion years of lunar bombardment. *Earth Planet. Sci. Lett.* 355–356, 144–151.

Morgan J. W., Ganapathy R., Higuchi H. and Anders E. (1977) Meteoritic material on the Moon. *Proc. Soviet Am. Conf. Cosmochemistry Moon Planets* 2, 659–689.

Morgan J. W., Walker R. J., Brandon A. D. and Horan M. F. (2001) Siderophile elements in Earth's upper mantle and lunar breccias: Data synthesis suggests manifestations of the same late influx. *Meteorit. Planet. Sci.* 36, 1257–1275.

Morgan J. W., Ganapathy R., Higuchi H., Krähenbühl U. and Anders E. (1974) Lunar basins: Tentative characterization of projectiles, from meteoritic elements in Apollo 17 boulders. *Proc. Lunar Sci. Conf.* 5, 1703–1736.

Morgan J. W., Laul J. C., Krähenbühl U., Ganapathy R. and Anders E. (1972) Major impacts on the moon: Characterization from trace elements in Apollo 12 and 14 samples. *Proc. Lunar Sci. Conf.* 3, 1377–1395.

Norman M. D. and Nemchin A. A. (2014) A 4.2 billion year old impact basin on the Moon: U-Pb dating of zirconolite and apatite in lunar melt rock 67955. *Earth Planet. Sci. Lett.* 388, 387–398.

Norman M. D. and Roberts J. (2013) Metal particles in Apollo 17 impact melt breccias: Textures and highly siderophile element

compositions. Lunar Planet. Sci. 44th. Lunar Planet. Inst., Houston. #1802(abstr.).
Norman M. D., Bennett V. C. and Ryder G. (2002) Targeting the impactors: siderophile element signatures of lunar impact melts from Serenitatis. *Earth Planet. Sci. Lett.* 202, 217–228.
Norman M. D., Duncan R. A. and Huard J. J. (2006) Identifying impact events within the lunar cataclysm from ^{40}Ar-^{39}Ar ages and compositions of Apollo 16 impact melt rocks. *Geochim. Cosmochim. Acta* 70, 6032–6049.
Norman M. D., Duncan R. A. and Huard J. J. (2010) Imbrium provenance for the Apollo 16 Descartes terrain: Argon ages and geochemistry of lunar breccias 67016 and 67455. *Geochim. Cosmochim. Acta* 74, 763–783.
Norman M. D., Taylor L. A., Shih C.-Y. and Nyquist L. E. (2016) Crystal Accumulation in a 4.2 Ga Lunar Impact Melt. *Geochim. Cosmochim. Acta* 172, 410–429.
Palme H. (1980) The meteoritic contamination of the terrestrial and lunar impact melts and the problem of indigenous siderophiles in the lunar highlands. *Proc. Lunar Planet. Sci. Conf.* 11, 481–506.
Palme H. and O'Neill H. S. C. (2003) Cosmochemical estimates of mantle composition. In *Treatise on Geochemistry 2* (eds. H. D. Holland and K. K. Turekian). Pergamon, Oxford, pp. 1–38.
Palme H., Spettel B., Wänke H., Borchardt R. and Stöffler D. (1982) Can metal segregation remove siderophiles from lunar impact melts? Lunar Planet. Sci. 13th. Lunar Planet. Inst., Houston. 609–610(abstr.).
Papanastassiou D. A. and Wasserburg G. J. (1972) Rb-Sr age of a crystalline rock from Apollo 16. *Earth Planet. Sci. Lett.* 16, 289–298.
Pernicka E. and Wasson J. T. (1987) Ru, Re, Os, Pt and Au in iron meteorites. *Geochim. Cosmochim. Acta* 51, 1717–1726.
Petaev M. I. and Jacobsen S. B. (2004) Differentiation of metal-rich meteoritic parent bodies: I. Measurements of PGEs, Re, Mo, W, and Au in meteoritic Fe-Ni metal. *Meteorit. Planet. Sci.* 39, 1685–1697.
Puchtel I. S., Walker R. J., James O. B. and Kring D. A. (2008) Osmium isotope and highly siderophile element systematic of lunar impact melt breccias: Implications for the late accretion history of the Moon and Earth. *Geochim. Cosmochim. Acta* 72, 3022–3042.
Rose-Weston L., Brenan J. M., Fei Y., Secco R. A. and Frost D. J. (2009) Effect of pressure, temperature, and oxygen fugacity on the metal-silicate partitioning of Te, Se, and S: Implications for earth differentiation. *Geochim. Cosmochim. Acta* 73, 4598–4615.
Schmitt W., Palme H. and Wänke H. (1989) Experimental determination of metal/silicate partition coefficients for P Co, Ni, Cu, Ga, Ge, Mo, and W and some implications for the early evolution of the Earth. *Geochim. Cosmochim. Acta* 53, 173–185.
Sharp M., Gerasimenko I., Loudin L. C., Liu J., James O. B., Puchtel I. S. and Walker R. J. (2014) Characterization of the dominant impactor signature for Apollo 17 impact melt rocks. *Geochim. Cosmochim. Acta* 131, 62–80.
Shen J. J., Papanastassiou D. A. and Wasserburg G. J. (1996) Precise Re-Os determinations and systematics of iron meteorites. *Geochim. Cosmochim. Acta* 60, 2887–2900.
Shirey S. B. and Walker R. J. (1998) The Re–Os isotope system in cosmochemistry and hightemperature geochemistry. *Annu. Rev. Earth Planet. Sci.* 26, 423–500.
Shuster D. L., Balco G., Cassata W. S., Fernandes V. A., Garrick-Bethell I. and Weiss B. P. (2010) A record of impacts preserved in the lunar regolith. *Earth Planet. Sci. Lett.* 290, 155–165.
Smoliar M. I., Walker R. J. and Morgan J. W. (1996) Re-Oa ages of group IIA, IIIA, IVA, and IVB iron meteorites. *Science* 271, 1099–1102.
Touboul M., Puchtel I. S. and Walker R. J. (2015) Tungsten isotopic evidence for disproportional late accretion to the Earth and Moon. *Nature* 520, 530–533.
Vaniman D. T. and Papike J. J. (1980) Lunar highland rocks: Chemistry, petrology and silicate mineralogy. *Proc. Conf. Lunar Highlands Crust*, 271–337.
Vaughan W. M., Head J. W., Wilson L. and Hess P. C. (2013) Geology and petrology of enormous volumes of impact melt on the Moon: A case study of the Orientale basin impact melt sea. *Icarus* 223, 749–765.
Walker R. J., Bermingham K., Liu J., Puchtel I. S. and Touboul M. (2015) In Search of the late-stage planetary building blocks. *Chem. Geol.* 411, 125–142.
Walker D., Grove T. L., Longhi J., Stolper E. M. and Hays J. F. (1973) Origin of Lunar feldspathic rocks. *Earth Planet. Sci. Lett.* 20, 325–336.
Wang Z. and Becker H. (2013) Ratios of S, Se and Te in the silicate Earth require a volatile-rich late veneer. *Nature* 499, 328–332.
Wang Z., Becker H. and Gawronski T. (2013) Partial re-equilibration of highly siderophile elements and the chalcogens in the mantle: A case study on the Baldissero and Balmuccia peridotite massifs (Ivrea Zone, Italian Alps). *Geochim. Cosmochim. Acta* 108, 21–44.
Wasson J. T. (1999) Trapped melt in IIIAB irons; solid/liquid elemental partitioning during the fractionation of the IIIAB magma. *Geochim. Cosmochim. Acta* 63, 2875–2889.
Wasson J. T., Huber H. and Malvin D. J. (2007) Formation of IIAB iron meteorites. *Geochim. Cosmochim. Acta* 71, 760–781.
Wetherill G. W. (1985) Asteroidal source of ordinary chondrites. *Meteoritics* 20, 1–22.
Wlotzka F., Jagoutz E., Spettel B., Baddenhausen H., Balacescu A. and Wä nke H. (1972) On lunar metallic particles and their contribution to the trace element content of Apollo 14 and 15 soils. *Proc. Lunar Sci. Conf.* 3, 1077–1084.
Yakovlev O. I., Dikov Yu. P. and Garasimov M. V. (2006) Experimental data on the thermal reduction of phosphorus and iron and their significance for the interpretation of the impact reworking of Lunar materials. *Geochem. Int.* 44, 847–854.

Associate editor: Richard J. Walker